Engineering Structures 366 (2026) 123271

Contents lists available at ScienceDirect

Engineering Structures

journal homepage: www.elsevier.com/locate/engstruct

Cold-formed shear walls with burring holes for the seismic strengthening of existing reinforced concrete buildings

Michelle Gualdi [a], Andrea Belleri [a,*], Simone Labò [a], Atsushi Sato [b]

[a] University of Bergamo, Department of Engineering and Applied Sciences, Dalmine, Italy
[b] Nagoya Institute of Technology, School of Engineering, Nagoya, Japan

ARTICLE INFO

Keywords:
Integrated renovation
Cold-formed steel panels
Seismic retrofit
Life cycle thinking
Existing RC structure

ABSTRACT

Decarbonization is a key priority in the global effort to promote sustainable development and mitigate climate change. A significant contribution can be made by renovating the existing European building stock, which is largely characterized by low energy efficiency and inadequate structural performance. To address this challenge, integrated and sustainable renovation strategies based on Life Cycle Thinking principles have been proposed, aiming to enhance both structural safety and energy performance. In this paper, cold-formed steel panels with burring holes are proposed as earthquake-resistant elements for the integrated renovation of existing reinforced concrete (RC) buildings. These shear walls are used in Japan as lateral force-resistant systems for new lightweight buildings. The proposed retrofit solution offers key advantages, including lightness, ease of installation, and the possibility of disassembly and component reuse, thereby enhancing overall sustainability. Three finite element modelling strategies with varying levels of complexity are presented to capture the behaviour observed in previous experimental campaigns. A design methodology for a retrofit solution for RC buildings is developed, incorporating the stringer-panel model to derive forces in individual elements. Finally, both the modelling approach and design method are validated through application to a reference case study building representative of existing RC structures not designed according to earthquake-resistant provisions. Vulnerability analyses have been performed, demonstrating the effectiveness of the designed retrofit solution involving perforated metal panels.

1. Introduction

In line with the main objective of the European Green Deal to achieve carbon neutrality by 2050, sustainability must become a priority in the development of all economic sectors, including construction. The construction sector is known to have significant environmental impacts, accounting for 40% of energy consumption and 36% of CO_2 emissions in Europe [1]. The European post-Second World War reinforced concrete (RC) building stock was primarily constructed to address the urgent housing demand of that period. Building materials often had poor performance, and non-specialized labourers lacked the necessary knowledge and experience, resulting in inadequate execution of structural and non-structural elements and leading to early obsolescence. Additionally, these structures were designed before the implementation of the first comprehensive codes for earthquake-resistant buildings. They are characterized by one-way RC frames with poor structural details and interacting masonry infills. Floors were typically made of one-way composite RC-masonry ribbed slabs, often without an RC overlay. A pilotis configuration at the ground floor was frequently used, introducing a significant discontinuity in stiffness and strength between stories. The considerable vulnerability of these buildings has been clearly demonstrated by the devastating effects of past earthquakes, which have caused substantial structural damage, economic losses, and human casualties. In Italy, the significant economic and social impacts of seismic events over the past 50 years have been highlighted by the Italian Department of Civil Protection [2]. In addition to their structural deficiencies, these buildings also have poor energy performance, further contributing to their overall obsolescence and underscoring the need for comprehensive assessment. Despite the clear structural and thermal deficiencies affecting these buildings, demolition and reconstruction are usually not sustainable options due to raw material depletion and hazardous waste production [3–5]. Currently, the renovation of existing RC buildings is typically addressed through limited and local interventions that do not resolve all the issues affecting the building, or it focuses only

* Corresponding author.
E-mail address: andrea.belleri@unibg.it (A. Belleri).

https://doi.org/10.1016/j.engstruct.2026.123271
Received 22 December 2025; Received in revised form 27 May 2026; Accepted 24 June 2026
Available online 2 July 2026

on energy aspects, such as external wall insulation or boiler replacement. However, the structural vulnerability of existing buildings, which can lead to severe damage during strong earthquakes, could significantly undermine the energy savings achieved through energy retrofit interventions alone [6].

In recent years, holistic renovations based on the principle of Life Cycle Thinking (LCT) have been proposed [7,8], aiming to address all building deficiencies through comprehensive interventions. The concept of LCT is applied to the design of retrofit solutions, with the goal of maximizing performance and minimizing environmental impacts and costs throughout the building's life cycle. The addition of an exoskeleton enhances both structural and energy performance and also improves the building's aesthetics. According to a World Bank analysis [9], earthquake prevention measures that include energy refurbishment are cost-effective and provide immediate benefits to inhabitants, even if a seismic event does not occur. Furthermore, the proposed intervention can be carried out entirely from the outside, allowing continuous use of the building and eliminating one of the main barriers to renovation: the need to relocate inhabitants. Retrofit solutions that use standardized and prefabricated elements optimize the installation process and improve the dismantlability of the system, thereby increasing its sustainability. Several configurations have been proposed as integrated solutions for building renovation, such as steel diagrid exoskeletons [10], prefabricated timber shell panels [11–14], two-dimensional orthogonal steel exoskeletons [15], and steel sandwich panels with structural and energy functions [16]. Other solutions include pin-supported walls [17, 18], which enable the linearization of frame deformation along the height and inhibit the development of a soft-storey collapse mechanism.

In this context, cold-formed steel (CFS) panels may be used as a structural layer in integrated renovation strategies. These shear walls are already widely employed worldwide as lateral force-resisting systems for new structures [19–21] due to their light weight, ease of installation, and favourable mechanical properties. Conversely, despite their potential, limited research has focused on the application of cold-formed steel members for the seismic energy retrofitting of masonry [22,23] and reinforced concrete buildings [24,25]. At the Nagoya Institute of Technology, a specific configuration of cold-formed steel panels with burring holes was proposed as a seismic-resistant system in new low- to mid-rise buildings. These shear walls consist of a thin steel sheet with burring holes aligned vertically, mechanically fastened to the frame members. The presence of burring holes enhances the out-of-plane stiffness and energy dissipation capacity of the panel, making the system suitable for resisting lateral seismic loads while maintaining light weight and ease of installation, key advantages in modern construction practices. Experimental and numerical investigations were conducted to determine the seismic behaviour and resistance mechanism, based on the concentration of stresses in the intervals between the holes [26–29]. These panels may also be coupled with steel rocking podium frames for new buildings or for the seismic retrofit of existing buildings, as preliminarily investigated in [30,31].

In this work, the effectiveness of CFS panels with burring holes for the integrated renovation of existing reinforced concrete buildings is assessed. The study aims to contribute to the development of a new type of sustainable exoskeleton for buildings, leveraging the advantages of prefabrication and standardization to expedite construction and reduce costs. The retrofit system is designed to be demountable, allowing for disassembly and reuse at the end of the building's nominal life, thus enhancing sustainability. Given the growing interest in lightweight steel solutions, it is significant that the current edition of Eurocode 8 (EN 1998) [32] lacks a dedicated section on cold-formed steel. Consequently, the design of such structures relies on the general provisions for hot-rolled steel elements, with necessary adaptations. The upcoming edition of EN 1998, to be released in the next few years, will introduce a specific section with design rules for lightweight steel systems [33]. This development reinforces the feasibility of CFS solutions for seismic design and will provide practitioners with practical design formulations. To evaluate the proposed system, this research combines numerical and analytical methods. Finite element (FE) models of the panel are developed to simulate the monotonic behaviour observed in previous experimental tests. An analytical design procedure involving the stringer-panel model is proposed to determine the optimal configuration of the retrofit system. A case study building is then analysed to validate both the modelling approach and the proposed design methodology. The paper is organized as follows: 2 provides an overview of the experimental background and the characteristics of the perforated CFS panel. 3 presents the development of three finite element modelling strategies. 4 outlines the analytical procedure proposed for the design of the retrofit system. In 5, the methodology is applied to a case study building, and the effectiveness of the intervention is evaluated through a vulnerability assessment of the building before and after the retrofit system is applied.

2. Panel characterization and experimental results

Steel sheet shear walls with burring holes are currently used as lateral force resisting systems in low- to -mid rise buildings in seismically active and typhoon-prone regions of Japan. Real applications of these shear walls are shown in Fig. 1. The burring holes are produced through a cold-pressing process. The standard configuration of these walls consists of 2.73 m-high and 0.91 m-wide sheets with 200 mm diameter holes aligned with a pitch of 321.6 mm, attached with self-drilling screws to vertical studs, rails and cross-rails made of cold-formed steel box and channel shapes with and without lips. The steel sheet is made of a zinc-aluminium-magnesium alloy-coated steel, JISG3323 SGMC400, with a nominal yield strength of 295 MPa (280 MPa is used for the design yield strength) and a nominal thickness of 1.2 mm. The four edges of the sheet are connected to the frame elements with 4.8 mm-diameter self-drilling screws spaced at 50 mm. The geometrical properties of the system are shown in Fig. 2, while the details of the cross-sections of the elements are summarized in Table 1. The distribution and dimensions of the burring holes (200 mm diameter with a 321.6 mm vertical pitch) follow the configuration previously developed and experimentally validated by Kawai et al. [26–29] for steel sheet shear walls with burring holes. This layout was shown to promote controlled stress localization in the steel sheet intervals between the holes and the development of stable diagonal tension fields, while the 10 mm curved burring ribs provide local out-of-plane stiffening that delays local buckling of the steel sheet intervals. The hole geometry was therefore maintained unchanged in the present study in order to preserve the experimentally validated mechanical behaviour of the system.

In terms of adaptability to existing RC buildings, the retrofit strategy relies on the modularity of the system rather than on customization of the hole size or spacing. Architectural compatibility is achieved by combining standard modular panels, introducing vertical slits for span adjustment, and varying the frame height according to the storey geometry. Therefore, the adaptability of the retrofit system is achieved through modular assembly while maintaining the reliability of the standardized components. Alternative panel geometries and hole layouts may be investigated in future studies through dedicated experimental and numerical validation.

The specimen was tested under cyclic loading in displacement control in a cantilever configuration with a point load applied at the top of the panel and both studs connected at the bottom to the testing frame through hold-down and anchor bolts. It was observed that under medium-to-large seismic loads, corresponding to the serviceability limit state, the walls exhibited stress concentrations in the intervals between the holes and displayed almost elastic behaviour. The primary failure mechanism was identified as local shear buckling of the steel sheet intervals between the burring holes, initiating at a storey drift angle of approximately 1/150 (Fig. 3, point 2). With increasing deformation, diagonal tension fields progressively developed within the sheet at a drift angle of approximately 1/100 (Fig. 3, point 3), allowing the panel

Fig. 1. Examples of real applications of steel sheet shear walls with burring holes.

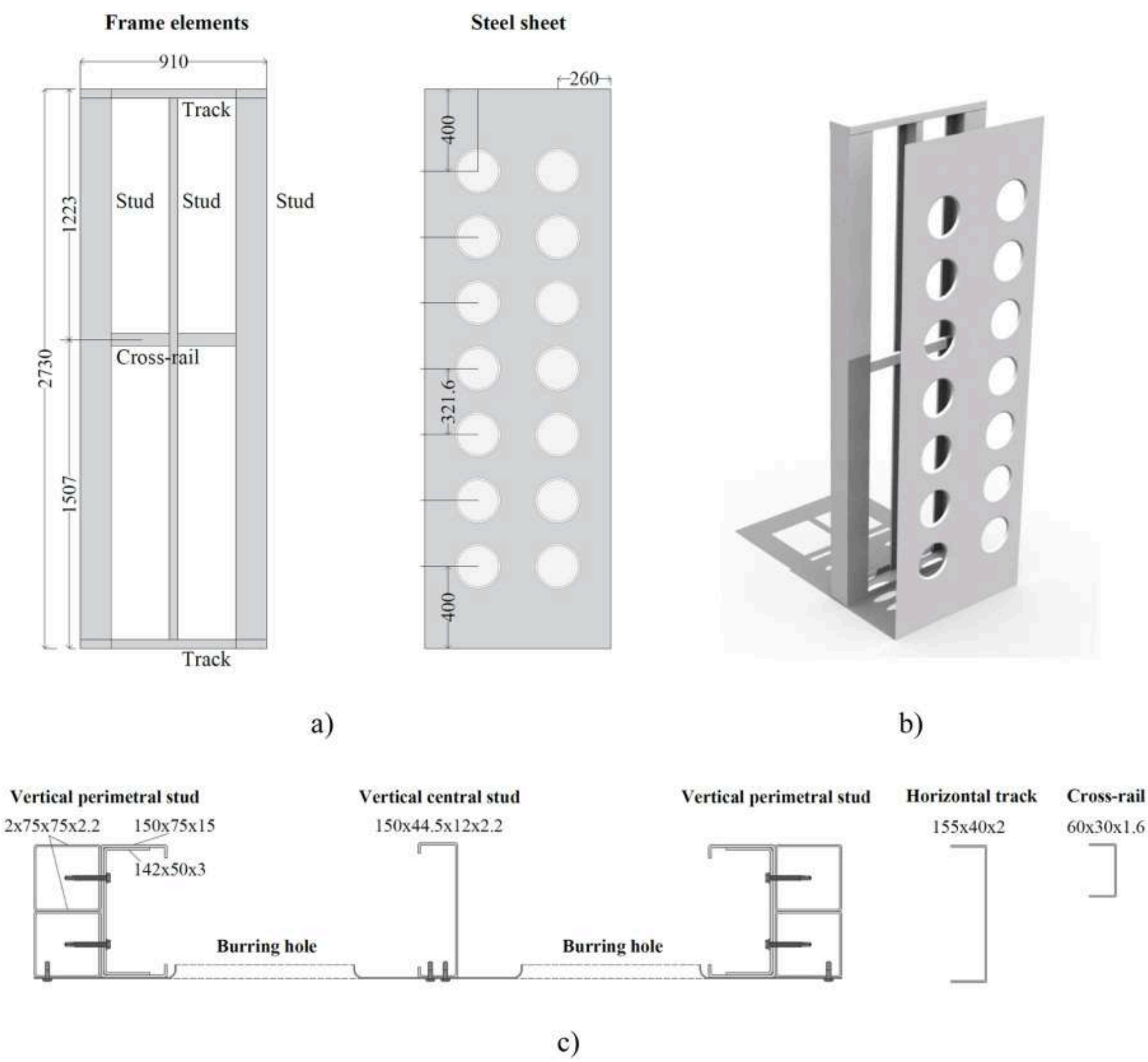

Fig. 2. a) Geometrical details of the frame elements and the steel sheet with burring holes (unit: mm), b) three-dimensional representation of the shear wall system and c) cross-sectional view of the panel with details of cold-formed profiles.

Table 1
Details of the cross-sections of the elements of the shear walls.

Element	Dimensions
Steel sheet with burring holes	Width: 455 mm; Height: 2730 mm; Thickness: 1.2 mm
Vertical perimetral studs	2 BOX: 75 × 75 x 2.2 mm + C: 150 × 75 x 15 × 3 mm + C: 142 × 50 x 3 mm
Horizontal tracks	C: 155 × 40 x 2.0 mm
Cross-rails	C: 60 × 30 x 1.6 mm
Vertical central stud	C: 150 × 44.5 × 12 x 2.2 mm

to maintain stable post-buckling lateral resistance, as shown by the hysteretic response in Fig. 3a. At larger deformation levels, the steel sheet exhibited progressive out-of-plane deformation, while the stiffened edges of the burring holes limited excessive local instability. The experimental observations showed that the inelastic response was primarily concentrated within the steel sheet intervals, whereas the surrounding frame members and screw connections remained effective in transferring forces without exhibiting dominant brittle failure mechanisms. Consequently, the global response was governed predominantly by structural instability and tension-field development rather than by material strain hardening. Based on the experimentally observed behaviour, an allowable design strength formulation was proposed in [29] to compute the seismic resistance as a function of the mechanical properties of the material and the geometrical characteristics of the intervals between the holes.

3. Numerical models

The first step of this research was the development of alternative shear wall models to provide tools with varying levels of complexity for different contexts. The first model, referred to as Model A, was developed using Simulia Abaqus [34] and is intended to capture stress concentrations in the regions between the holes and reproduce the system's monotonic behaviour. The second and third models, referred to as Model B and Model C, were developed in the commercial software MidasGen [35], with decreasing levels of complexity. Model B uses shell elements with plastic behaviour, while Model C, the simplest model, employs elastic beam elements. In Model C, the inelastic behaviour of the panel is represented through calibrated concentrated plasticity. The conceptual schemes of the three models are illustrated in Fig. 4. The purpose of these numerical investigations, in addition to replicating the experimental behaviour, is to develop a practical tool for professional engineers modelling this type of panel for the seismic retrofit of existing buildings.

3.1. Model A

3.1.1. Model definition and nonlinear static analysis

The first model, Model A, was developed using Simulia Abaqus and accounted for geometric nonlinearities. The conceptual scheme of the model is shown in Fig. 4a. Frame elements were modelled as elastic beam elements (E = 210000 MPa) and pin-connected to each other. The two 0.455 m-wide sheets with burring holes were modelled using continuum shell elements with an elastic perfectly plastic material (E = 210000 MPa, σ_y=295 MPa). The out-of-plane lips of the burring holes were explicitly modelled in Model A to account for the localized stiffness effects associated with the burred geometry. Furthermore, a non-uniform mesh strategy with local refinement around the holes and along the burred edges was adopted to adequately capture the stress distribution and local buckling patterns observed experimentally. The frame was connected to the ground through two absolute pinned supports located at the lower corners. Out-of-plane constraints were imposed on all frame elements to simulate the restraining effect of the existing structure. Beam and shell elements were connected through nonlinear spring cartesian-type connectors spaced at 50 mm, consistently with the screw spacing adopted in the experimental specimen. The connectors were assigned an elasticity and plasticity behaviour with a nonlinear shear-slip constitutive law derived from the experimental characterization of the self-drilling screw connections reported by Kawai et al. [26–29]. The value of 6800 N/mm corresponds to the initial elastic stiffness of the connector response. No explicit connector fracture criterion was introduced, as the experimental tests showed that the global response was governed by local shear buckling and tension-field development in the steel sheet, while the screw connections remained effective in transferring forces even at large panel displacements. In the out-of-plane direction, rigid connector behaviour was assumed to reproduce the experimental restraint conditions and prevent artificial separation between the sheet and the frame.

To ensure consistency with the experimental setup described in 2, the horizontal action was applied to the upper track of the panel and uniformly distributed to its nodes through displacement-controlled loading. A preliminary linear buckling analysis was performed in Abaqus to identify the dominant local instability modes of the steel sheet. A

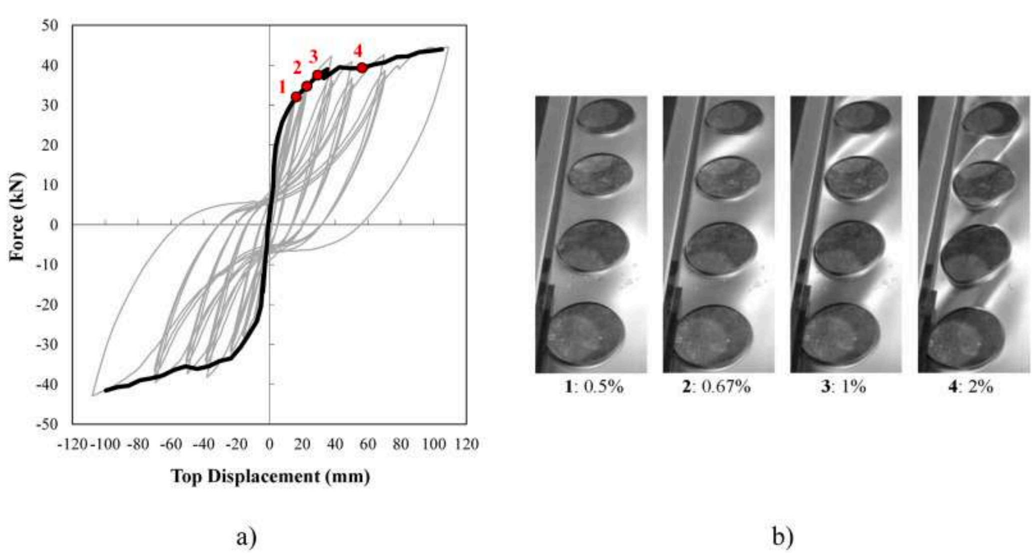

Fig. 3. a) Experimental hysteresis loops and envelope curve used for numerical analyses; b) visual evolution of the steel sheet buckling and diagonal tension field development at different drift levels (adapted from [26]).

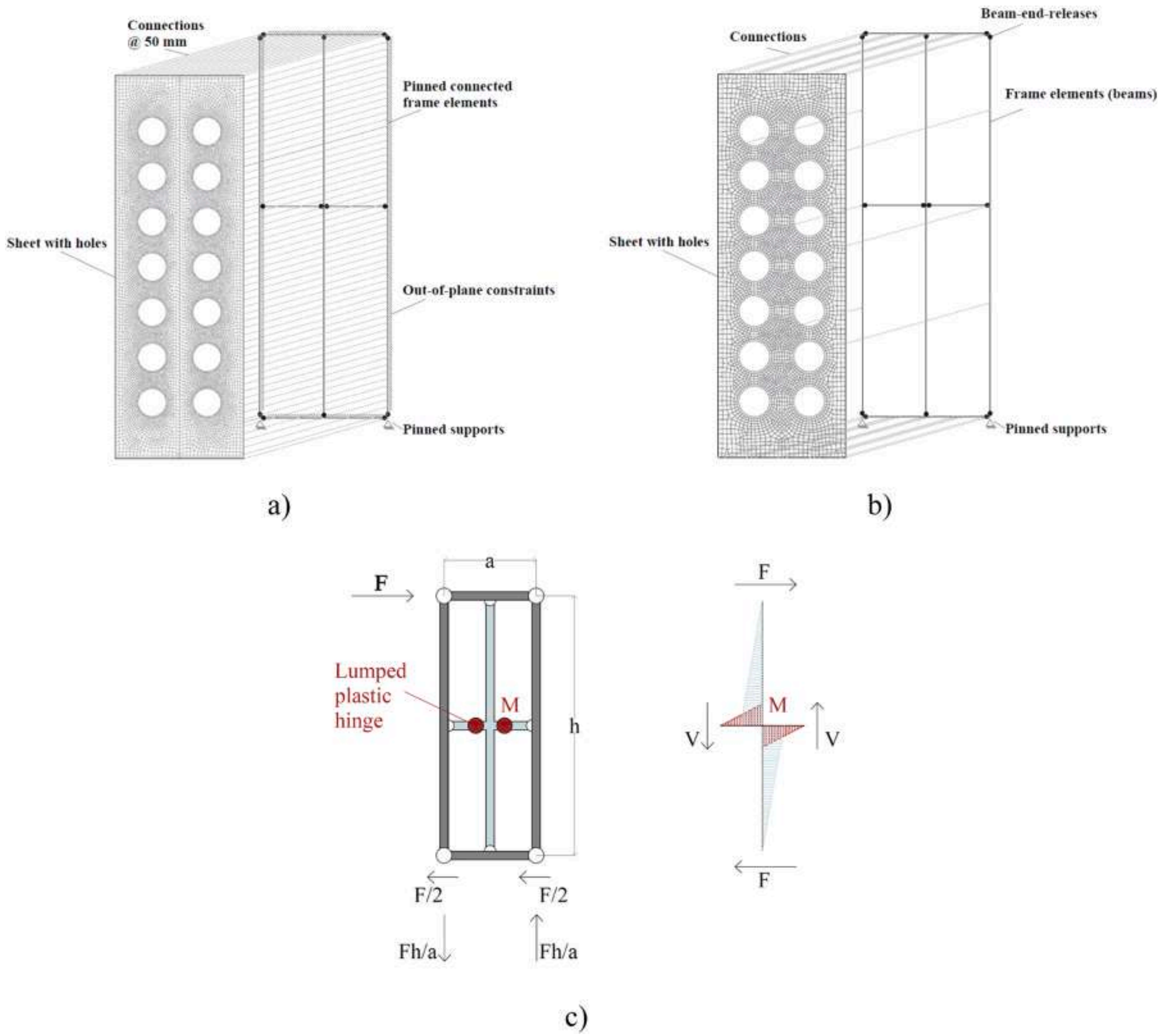

Fig. 4. Conceptual scheme of a) Model A, b) Model B and c) Model C.

combination of the first four buckling modes was subsequently introduced with equal weights as an initial geometric imperfection in the nonlinear static analysis to trigger the experimentally observed instability mechanisms. A mesh sensitivity analysis was also conducted to evaluate the influence of shell discretization on the numerical response. Different mesh densities were investigated, with local refinement adopted in the regions surrounding the burring holes to accurately capture stress localization and local buckling phenomena. The final mesh configuration was selected after verifying the convergence of the global force-displacement response and the plastic strain localization patterns, while maintaining a satisfactory balance between numerical accuracy and computational demand. A nonlinear static analysis, using the "*Static, General*" procedure, was carried out until a displacement of 105.16 mm was reached. The monotonic force-displacement curve obtained from the analysis is shown in Fig. 8, where it is compared with the experimental curve. By analysing the two curves, it was observed that the numerical model accurately reproduces the experimental behaviour of the shear wall under testing conditions. The yielding point closely coincides in both cases, while the ultimate resistance is slightly overestimated in the numerical simulation. The numerical model was able to reproduce the dominant failure mechanisms observed during the experimental tests. As the imposed displacement increased, stress and strain localization developed within the steel sheet intervals between the burring holes (Fig. 5). The simulations reproduced the development of the tension-field mechanism together with the associated local buckling patterns observed experimentally. At large displacement levels, significant out-of-plane deformations developed within the steel sheet, confirming the influence of the burring holes on the instability mode shapes. Furthermore, the connector elements exhibited nonlinear deformation behaviour while remaining effective in transferring forces between the steel sheet and the surrounding frame.

The apparent post-elastic hardening observed in both the experimental and numerical responses is not related to material strain hardening, since the steel sheet was modelled with an elastic-perfectly plastic constitutive law. Instead, this behaviour is associated with the progressive development of tension-field actions within the steel sheet and the consequent activation of the flexural contribution of the boundary studs through the nonlinear screw connections.

3.1.2. Parametric analysis and design formulations

(a) Resistance and elastic stiffness

Following the validation of the numerical model, a sensitivity analysis was conducted to investigate the influence of the steel sheet thickness (t) on the mechanical properties of the panel. The thickness was varied from 1 mm to 2 mm with increments of 0.1 mm, while the stiffness and strength of the connections were calibrated proportionally for each configuration. The resulting force-displacement curves are illustrated in Fig. 6a. The primary objective of this analysis was to derive analytical formulations for both the shear resistance and the initial elastic stiffness as a function of the sheet thickness. These expressions serve as a practical design tool, enabling an informed selection of the panel properties based on the target design capacity. The design shear

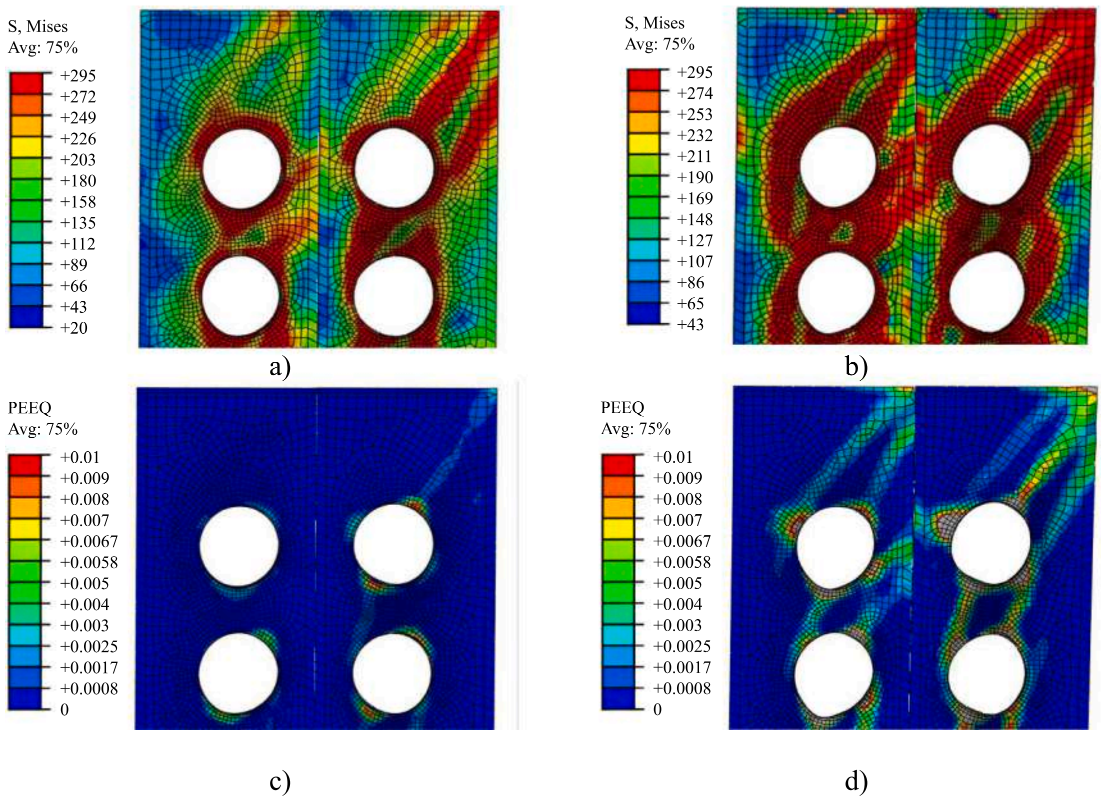

Fig. 5. Numerical results at 20 mm (0.7% drift) and 54.6 mm (2% drift) displacements: (a-b) Von Mises stress in MPa and (c-d) Equivalent Plastic Strain (PPEQ).

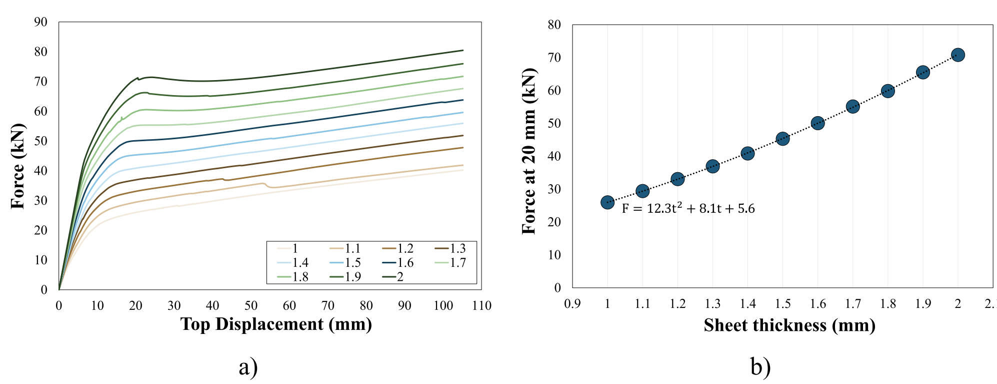

Fig. 6. a) Numerical force-displacement curves for Model A with varying sheet thickness and b) shear strength of the panel at 20 mm and result of the regression analysis.

resistance (F_{20}) was calibrated at a top displacement of 20 mm, corresponding to a drift ratio of 0.7%. Experimental observations showed that this deformation level marks the onset of significant shear buckling and stiffness degradation within the burring holes intervals. Consequently, F_{20} was adopted as a design-oriented resistance threshold representative of the transition between predominantly elastic behaviour and the onset of post-elastic instability and yielding mechanisms. The proposed formulation is intended to support the retrofit design procedure by determining the required sheet thickness as a function of the target seismic demand. A quadratic polynomial regression was performed to correlate the shear resistance with the thickness, yielding the following expression (where t is in mm and F_{20} in kN):

$$F_{20} = 12.3t^2 + 8.1t + 5.6 \tag{1}$$

As expected, the initial elastic stiffness (k_{el}) followed a linear trend with respect to the thickness. The resulting formulation (with k_{el} in kN/mm) is:

$$k_{el} = 4t - 1.3 \tag{2}$$

It should be noted that Eq. (1) represents an empirical design-oriented relationship calibrated for the specific panel configuration investigated in this study, in which the geometry and arrangement of the burring holes were kept constant. Within the proposed retrofit methodology, the steel sheet thickness represents one of the most direct and practically adjustable parameters for calibrating the lateral strength and stiffness of the panel according to different seismic demands. For this reason, the parametric investigation was intentionally focused on the variation of sheet thickness within the investigated range. Additional sensitivity analyses showed that variations in the flexural stiffness of the boundary studs mainly influence the post-elastic response, while the panel resistance at the selected yielding threshold remains only marginally affected. Consequently, Eq. (1) should be considered valid for the investigated range of sheet thicknesses and panel geometries adopted in the present study.

(b) Influence of stud stiffness on post-elastic behaviour

During the numerical simulations, it was observed that the post-elastic hardening behaviour of the panel is predominantly influenced by the flexural contribution of the vertical boundary studs. In particular, variations in the second moment of inertia of the studs (I_{studs}) mainly affected the post-yield stiffness and the ultimate resistance of the panel, while the initial elastic stiffness and the design resistance evaluated at the conventional yielding displacement remained only marginally affected.

In practical retrofit applications, it may become necessary to increase the stud dimensions or adopt alternative stud cross-sections to satisfy stud buckling verifications. Consequently, an additional sensitivity analysis was conducted by progressively increasing the stud inertia up to four times the reference configuration. Based on the obtained numerical results, a corrective coefficient β was derived to account for the influence of stud stiffness on the post-elastic response:

$$\beta = \frac{k_{post,rev}}{k_{post,standard}} = 1 + (1.35 - 0.61t)\cdot \ln(n) \tag{3}$$

where n is the ratio between the modified and reference stud inertia values.

The results showed that the influence of stud stiffness becomes progressively less significant as the sheet thickness increases. Furthermore, the sensitivity analysis highlighted that the variation of stud stiffness produces only limited modifications of the design resistance F_{20} (e.g., approximately 5% for a 1.2 mm sheet with doubled stud inertia). The applicability of the formulation should be interpreted within the investigated range of panel geometries, sheet thicknesses and stud inertia values.

3.2. Model B

Based on the experimental data and test setup, a second modelling approach was developed in MidasGen to reproduce the global experimental response through a simplified shell-based finite element formulation. In a previous study by Gualdi et al. [36], various different FE models were preliminary investigated using this software, each with increasing complexity, to identify a modelling strategy suitable for practical engineering applications. For brevity, only the final calibrated configuration adopted in the present study is presented here. The steel sheet was modelled using plastic plate elements with a uniaxial yield stress of 295 MPa and a thickness of 1.2 mm. Frame members were modelled as elastic beam elements, pin-connected to each other. A nominal Young's modulus of 210000 MPa was assigned to all elements. Holes without burring were inserted in the model at their actual positions, and two pinned supports were attached to the base. A quad-dominated shell mesh consistent with the discretization strategy adopted in Model A was used. Unlike Model A, the connections between the steel sheet and the surrounding frame were represented through an equivalent simplified arrangement of rigid links, whose number and distribution were calibrated to reproduce the global experimental force-displacement response. The conceptual scheme of Model B is shown in Fig. 4b.

To obtain the capacity curve, a nonlinear static analysis was performed by controlling the displacement of the centre of the highest part of the plate. As in Model A, the maximum allowable displacement was set at 105.16 mm, corresponding to the displacement capacity observed in the experimental test. As shown in Fig. 8, Model B provides a satisfactory representation the global experimental force-displacement response.

Unlike Model A, Model B does not explicitly include geometric imperfections or out-of-plane instability effects. Consequently, the compression stress paths remain active during loading and the stress redistribution associated with local buckling phenomena is not directly reproduced. Therefore, the local stress distribution obtained from Model B should not be interpreted as physically representative of the actual local instability mechanisms occurring in the steel sheet. To compensate for this simplification and achieve consistency with the observed global behaviour, the number and arrangement of the connectors between the plate and frame elements were calibrated. Specifically, 11 connections were adopted along the horizontal tracks and 5 along the vertical boundary studs.

Compared to the refined Abaqus model, this shell-based approach significantly reduces modelling complexity and computational demand while remaining implementable within a commercial structural analysis software commonly used in engineering practice. The main objective of Model B is not the accurate reproduction of local stress or instability phenomena, but rather the development of a simplified engineering-oriented model capable of reproducing the global lateral response of the panel system with reduced computational effort. However, despite its simplified formulation, Model B still requires a non-negligible computational effort for large-scale structural analyses. For this reason, a further simplified macro-model (Model C) was subsequently developed.

3.3. Model C

To provide a computationally efficient tool for large-scale structural simulations, a simplified macro-element model, denoted as Model C, was developed using MidasGen. While Model A and Model B rely on refined shell discretization, Model C is based on an equivalent beam-based framework. The objective of this approach is to reproduce the global force-displacement response of the panel through a simplified formulation suitable for engineering-oriented structural analyses, without explicitly modelling local instability phenomena.

3.3.1. Model definition

Model C is characterized by a dual-component assembly with beam elements:

- Boundary frame: the external studs and tracks modelled with elastic beam elements, pin-connected to each other;
- Equivalent bracing system: the steel sheet, represented through cross-arranged beam elements pinned to the boundary studs.

The post-elastic response of the panel, including the effects associated with shear buckling and tension-field development within the steel sheet, is phenomenologically reproduced through lumped plastic hinges located at the midspan of the internal horizontal members, at the intersection between the internal horizontal and vertical members. As illustrated in Fig. 4c, the geometry of the equivalent internal mechanism induces a linear bending moment distribution within the elements, with maximum bending demand occurring at midspan, where the calibrated hinges were introduced.

3.3.2. Elements calibration and general applicability

The cross-section of the internal cross-arranged elements was calibrated to reproduce the initial elastic stiffness of the panel (k_{el}) observed experimentally. The equivalent second moment of inertia (I) required for the cross-arranged elements is therefore:

$$I = \frac{k_{el}h^2(a+h)}{12E} \tag{4}$$

where a and h are the width and the height of the panel, respectively.

To ensure consistency between the analytical formulation and the numerical response of the macro-model, the external studs are modelled as axially rigid members. The nonlinear response is introduced through a trilinear moment-rotation (M-θ) hinge law (Fig. 7). The characteristic

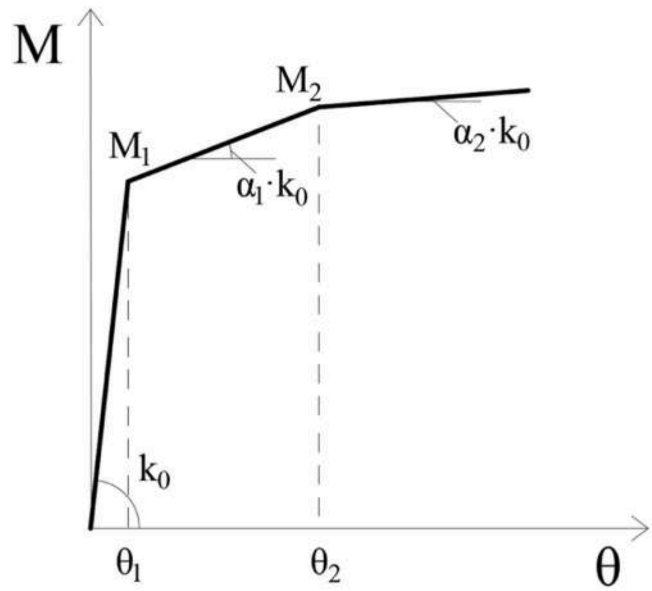

Fig. 7. Trilinear skeleton curve for plastic hinges in Model C.

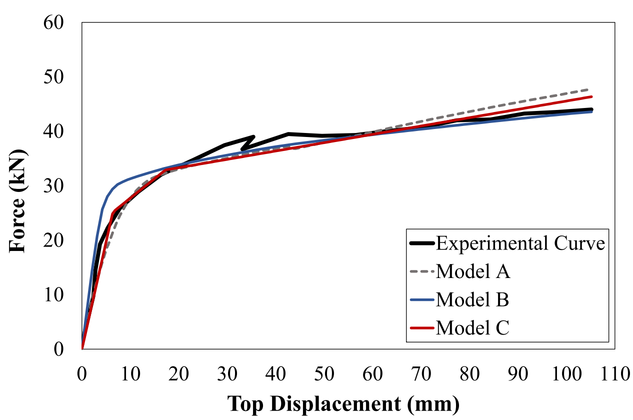

Fig. 8. Comparison between experimental and numerical force-displacement curves.

hinge moments (M_1 and M_2) are derived from the panel shear resistance (F) through the equilibrium relation $M=F \bullet h/2$. The observed stiffness degradation is incorporated through the reduced post-elastic stiffness branches defined by the coefficients α_1 and α_2. The elastic rotational stiffness (k_0) of the plastic hinges is computed as $3EI/(a/2)$.

The calibration procedure integrates the analytical regression laws derived in 3.1. (Eqs. 1, 2, 3), allowing the model to be adapted to different sheet thicknesses and stud cross-sections within the investigated ranges. Although local mechanisms are not explicitly reproduced, Model C provides an accurate phenological representation of the global panel response with significantly reduced computational demand compared to refined shell-based models.

4. Methodology for the design of a retrofit system with panels

This section presents an iterative methodology for the design of retrofit interventions based on cold-formed steel panels for existing RC buildings. The proposed approach combines spectrum-based seismic analysis, equivalent lateral force distributions and simplified analytical formulations to provide a practical design-oriented procedure suitable for engineering applications.

The methodology was developed with reference to low-rise RC residential buildings within the investigated range of panel geometries and sheet thicknesses. The design philosophy assumes that the CFS panels provide the primary contribution to the lateral stiffness and strength of the retrofitted building to limit interstorey drift demand and reduce damage concentration in the existing RC frame and masonry infills. For buildings characterized by severe torsional irregularities, highly non-uniform stiffness distributions or very high seismic demand, additional detailed analyses and potentially alternative retrofit strategies may be required. Since the retrofit intervention modifies the global stiffness distribution and modal properties of the structure, the final retrofitted configuration needs to be verified through detailed modal and nonlinear analyses.

The proposed methodology consists of four steps. In Step 1, a preliminary sizing of the retrofit system is performed based on spectrum analysis. In Step 2, the strength of the retrofit system is analytically derived, while Step 3 involves a preliminary global assessment in the Acceleration-Displacement Response Spectrum (ADRS) domain through an equivalent SDOF representation of the retrofitted building. Finally, in Step 4, the stringer-panel model (SPM) is employed to evaluate the internal force distribution and perform member-level buckling verifications of the CFS components.

4.1. STEP 1: spectrum analysis and preliminary sizing

The seismic input is determined according to Eurocode 8 [32] provisions through the horizontal response spectrum corresponding to the life safety limit state. For the investigated class of low-rise RC buildings, the fundamental periods are typically relatively short and the retrofitted configurations generally remain within the constant-acceleration region of the response spectrum. The seismic base shear force F_b is evaluated as:

$$F_b = S_d(T_1) \cdot m \cdot \lambda \tag{5}$$

where m is the total mass, λ is the correction factor for the number of storeys. A behaviour factor equal to 1.5 is adopted to account for the limited ductility capacity of the existing RC structure. The lateral forces are distributed along the height assuming a first-mode proportional distribution of the retrofitted configuration:

$$F_i = F_b \cdot \frac{z_i \cdot m_i}{\sum z_j \cdot m_j} \tag{6}$$

where z_i and m_i are the height and mass associated with the i-th storey.

At this preliminary stage, the retrofit panels are sized assuming that they provide the primary contribution to the lateral stiffness and strength of the retrofitted structure. This assumption is intentionally adopted as a conservative drift-control-oriented criterion aimed at limiting deformation demand and damage concentration within the existing RC frame and masonry infills. If the steel sheet thickness is predefined, the required number of panels is estimated by dividing the storey shear demand by the design panel resistance F_{20}. Alternatively, the number and arrangement of panels may first be selected according to geometric and architectural constraints, while the corresponding sheet thickness is subsequently determined. A double-panel configuration may also be adopted when the required resistance exceeds the capacity achievable through a single-sheet solution within the investigated thickness range. In this configuration, perforated steel sheets are installed on both sides of the same CFS frame. Within the proposed simplified modelling approach, the two sheets are assumed to act in parallel, resulting in approximately doubled values of both the elastic stiffness k_{el} and the design resistance F_{20}, while the post-elastic stiffness is conservatively assumed to remain unchanged since the hardening response is primarily governed by the flexural stiffness of the boundary studs.

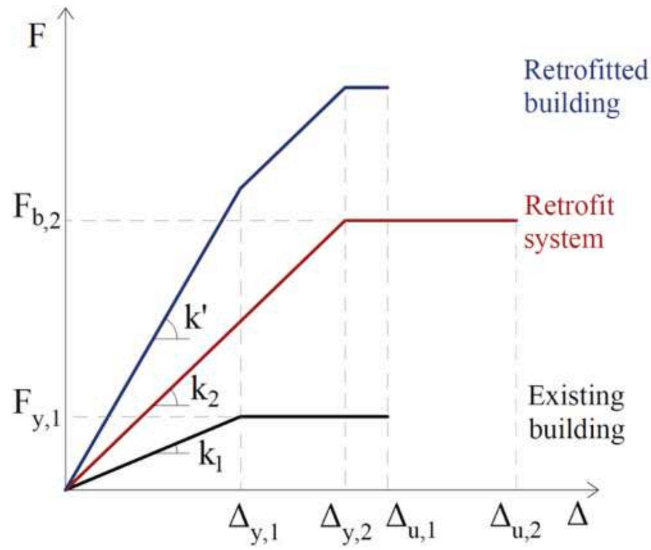

Fig. 9. Backbone curves of the three considered systems.

4.2. STEP 2: evaluation of the retrofit system capacity

The equivalent stiffness of the retrofit system is evaluated by assuming that the panels installed at each storey act in parallel. The total lateral stiffness at the i-th storey is therefore:

$$k_i = \sum_{j=1}^{n} k_{i,j} \tag{7}$$

where $k_{i,j}$ is the elastic stiffness of the j-th panel at the i-th storey.

Given the storey shear force V_i derived from Step 1, the storey displacement is estimated as:

$$\Delta_i = \frac{V_i}{k_i} \tag{8}$$

The total roof displacement, Δ_{roof}, is obtained by the summation of the individual storey displacements. The equivalent global stiffness of the retrofit system, k_2, is then defined as:

$$k_2 = \frac{F_b}{\Delta_{roof}} \tag{9}$$

The global lateral resistance of the retrofit system is estimated assuming that the response is governed by the panels installed at the first storey:

$$R_{sys} = \sum_{j=1}^{n} F_{20,j} \tag{10}$$

where $F_{20,j}$ is the design shear resistance of the j-th panel evaluated through Eq. 1.

It should be noted that the proposed formulations represent simplified analytical estimates intended for preliminary retrofit sizing within the investigated range of panel configurations.

4.3. STEP 3: global assessment of the retrofitted structure

The retrofitted building is subsequently represented through an equivalent SDOF system to perform simplified global performance checks within the ADRS domain.

Assuming rigid connections between the retrofit panels and the RC structure, the initial stiffness of the retrofitted system is evaluated as the combination of the stiffness of the existing structure k_1 and the retrofit contribution k_2. The structural response is represented through a simplified trilinear backbone curve (Fig. 9) describing the initial elastic response of the combined system, the post-yield response after activation of the existing RC frame nonlinearities, the subsequent nonlinear response governed by the retrofit panels. Following a low damage design approach, herein the retrofit configuration is considered satisfactory if the interstorey drift demand at the LSLS remains below the target value of 0.3%, selected to limit damage to non-structural components [37]. In this step of the procedure, it is recommended that the retrofit stiffness k_2 is at least 1.5 times greater than k_1.

The proposed methodology follows an iterative refinement process. If the target drift performance is not achieved, the retrofit configuration is modified by increasing the number or stiffness of the panels. Conversely, if the retrofit system appears excessively over-resistant, the panel configuration can be recalibrated by redistributing the seismic forces between the retrofit system and the existing structure according to their relative stiffness contributions. The final retrofit solution must always be verified through detailed modal analyses and nonlinear static analyses of the complete retrofitted structure.

4.4. STEP 4: stringer-panel model for the distribution of forces among elements

The SPM is adopted as the final step of the proposed design procedure to evaluate the internal force distribution within the CFS panels. Originally developed for aeronautical engineering [38–40], and later extended to structural reinforced concrete [41] and seismic diaphragm design [42,43], the SPM decomposes planar systems into one-dimensional stringers resisting axial forces and two-dimensional panels transferring shear flows. According to equilibrium, the shear transfer at the panel-stringer interface produces a linear variation of axial forces within the stringers. While the global design procedure defines the required panel configuration, the SPM allows the internal forces acting on studs and cross-rails to be estimated in a computationally efficient manner. Once the axial demands (N_{Ed}) acting on studs and cross-rails have been determined, member-level buckling verifications can be performed according to the Eurocode 3 provisions for cold-formed steel elements (EN 1993–1–1, EN 1993–1–3 and EN 1993–1–5) [44]. This approach allows the local instability mechanisms governing the steel sheet behaviour to be treated separately from the global instability verification of studs and tracks. Fig. 10 illustrates the application of the method to a three-storey configuration. Internal studs located between adjacent panels are subjected to equal and opposite axial forces generated by the shear flows, resulting in negligible net axial demand under horizontal loading.

5. Application to a case study

The numerical modelling strategy and the proposed design procedure were validated by applying them to a reference case study building that exhibits typical features of European buildings from the 1970s and 1980s. The selected case study is a residential three-storey building with a rectangular shape (15.8 m x 7.88 m). The reference plan and elevation of the case study building are shown in Fig. 11. The load-bearing structure, which was not designed to withstand seismic actions, consists of RC beams and columns. Seismic actions are resisted by three longitudinal frames and two transverse frames at the perimeter. The interstorey height is 2.6 m at the ground floor and 3.1 m at the upper floors, for a total height of 8.8 m. The frame spans are 3.0 m and 3.4 m in the longitudinal direction, and 3.45 m and 4.43 m in the transverse

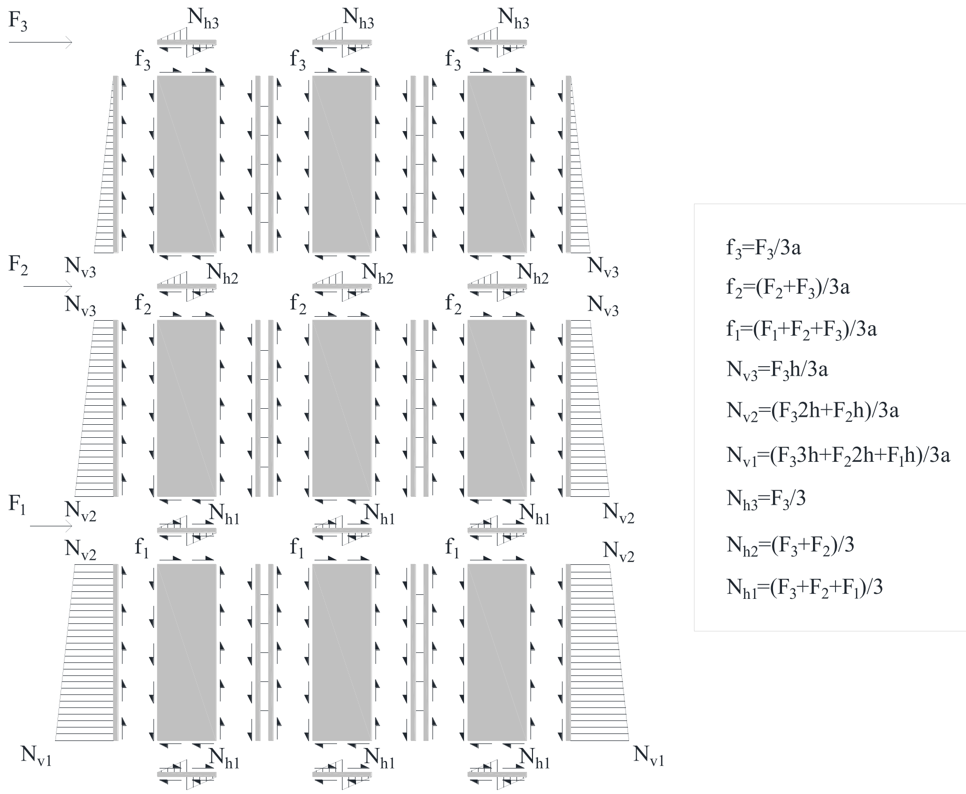

Fig. 10. Example of application of stringer-panel model for the analytical computation of internal forces in cold-formed steel panels. Note: *h* and *a* stand for height and width of the panels respectively.

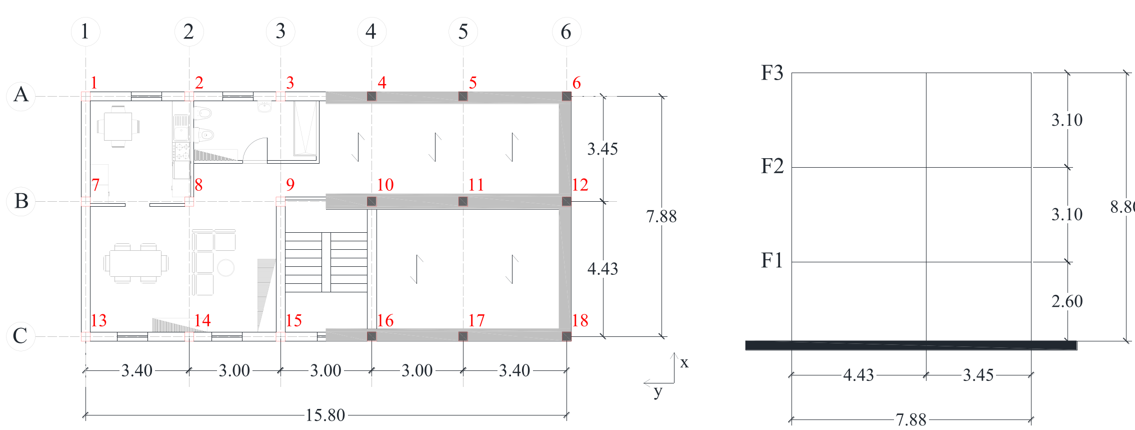

Fig. 11. Characteristics of the reference case study building: plan and elevation (unit: m).

direction. The floors are made of a one-way composite RC beam-and-clay-block system with a 3 cm RC overlay, for a total thickness of 19 cm. The staircase consists of stepped inclined beams. Details of the cross-sections of the structural elements are provided in Appendix A. For the non-structural elements, the perimeter masonry infills consist of two layers of hollow brick with two outer layers of plaster, corresponding to the medium infill described in [45]. In accordance with the codes in effect at the time of construction, concrete C20/25 ($f_{ck} = 20$ MPa) and steel FeB32K ($f_{yk} = 315$ MPa, $f_{tk} = 490$ MPa) were used. Live loads (Q) were assumed to be 2 kN/m^2, as required by the Italian Building Code (NTC18) [46]. For intermediate floors, the dead load of both structural (G_1) and non-structural (G_2) components was 2.5 kN/m^2, while for the non-accessible roof, the total dead load ($G_1 + G_2$) was 3.6 kN/m^2.

5.1. Numerical analysis of the structural response

A three-dimensional numerical model of the building was developed in MidasGen, with the structural frame idealized using beam elements. Inelastic behaviour was captured through lumped plastic hinges, with flexural and shear responses defined according to Eurocode 8 backbone curves. For RC columns, a P–M–M interaction-based hinge formulation was adopted to dynamically update the flexural capacity according to

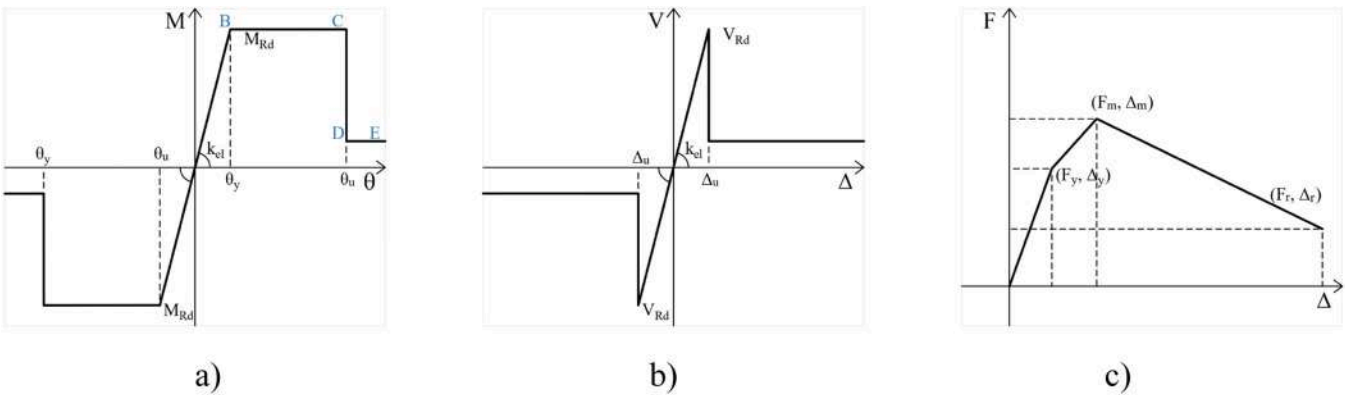

Fig. 12. Lumped plastic hinge characteristics: a) flexural behaviour, b) shear behaviour; c) axial behaviour of the compression-only diagonal struts.

the varying axial load during the nonlinear analysis. Specifically, the flexural behaviour was modelled using an elastic-perfectly-plastic bilinear curve (Fig. 12a). The shear plastic hinge exhibits a linear response up to its ultimate capacity, after which an abrupt strength degradation occurs, representing brittle failure (Fig. 12b). The characteristic points of both flexural and shear response curves were computed according to Eurocode 8 formulations. To account for cracking effects, the stiffness of beams and columns was reduced by 50% and 30%, respectively, to account for concrete cracking.

Masonry infills were modelled through the equivalent diagonal strut approach using compression-only truss elements. The equivalent cross-sectional area of the struts was evaluated according to the formulations proposed by Decanini et al. [47], and Sassun et al. [48]. The nonlinear axial behaviour of the infills was represented through a trilinear force-displacement (*F-Δ*) constitutive law accounting for cracking, peak resistance and residual strength (Fig. 12c). The cracking force and peak strength were evaluated according to the approach proposed by Decanini et al. [47], while the corresponding drift values were set to the commonly adopted thresholds of 0.3% for minor cracking (Δ_x), 0.5% for peak capacity (Δ_y), and 1.86% for residual strength (Δ_r) [48]. The adopted modelling parameters are summarized in Table A3 in Appendix. Infill panels with openings were not modelled, as their influence on the global resistance and stiffness of the building was assumed to be negligible. The floor slabs were assumed to effectively transfer horizontal loads and were therefore modelled as rigid diaphragms.

The seismic performance of the existing building was assessed using nonlinear static analyses conducted along the two principal directions of the structure. Hereafter, the transverse and longitudinal directions are referred to as the X and Y directions, respectively. The capacity curve in the weaker direction, the X direction, is shown in Fig. 13a. The performance evaluation considered two structural limit states defined by the Italian Building Code [45]. A nominal design life of 50 years and importance class II were adopted for the building. Specifically, the Life Safety Limit State (LSLS), associated with a 10% probability of exceedance within the reference period (corresponding to a 475-years return period), and the Collapse Prevention Limit State (CPLS), associated with a 5% probability of exceedance (975-years return period), were considered. In addition, the Immediate Occupancy Limit State (IOLS, 30-years return period) and the Serviceability Limit State (SLS, 50-years return period) were included in the vulnerability assessment. The CPLS is defined as the point where the structural strength decreases by 15%

Table 2
N2 method main parameters for the existing structure for the X direction.

Parameter	Symbol	Unit	Value
Participation factor	Γ	(-)	1
Mass of the equivalent SDOF system	m	kN/g	390
Fundamental period of the equivalent SDOF system	T_1	s	0.60
Stiffness of the equivalent SDOF system	k_1	kN/m	54003
Yielding force of the bilinear curve	F_{y1}	kN	579
Yielding displacement of the bilinear curve	d_{y1}	m	0.014
Displacement capacity of the SDOF system for the Life Safety (LS) limit state	d_c^{LS}	m	0.031
Displacement capacity of the SDOF system for the Collapse Prevention (CP) limit state	d_c^{CP}	m	0.042
Displacement demand for the SDOF system for the LS limit state	d_d^{LS}	m	0.039
Displacement demand for the SDOF system for the CP limit state	d_d^{CP}	m	0.049

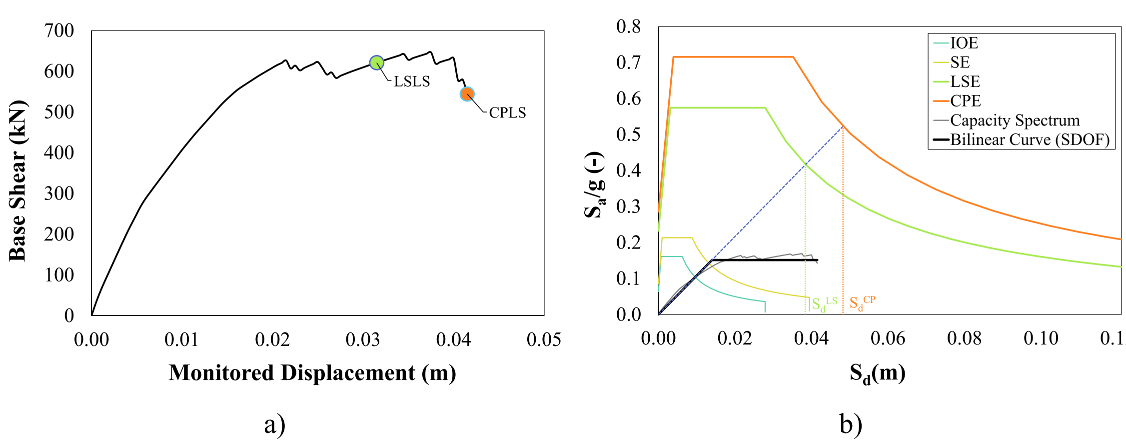

Fig. 13. a) Capacity curve of the existing building in the X direction and b) vulnerability analysis in the ADRS for various limit states with their return period.

from its peak value, while the LSLS is set at three-quarters of the CPLS displacement. The SLS capacity is defined as the minimum displacement corresponding to the maximum shear of the bilinear curve and the maximum shear of the multi-degree-of-freedom curve. The capacity at IOLS is set at two-thirds of the SLS capacity. For the seismic demand, the building was assumed to be located in Toscolano Maderno, Italy, with a peak ground acceleration of $a_g = 0.105$ g and a soil type C. In accordance with the Italian building code, the vulnerability assessment was conducted using the N2 method [49]. Two different lateral force distributions were considered for each direction: a multimodal distribution, which accounts for higher modes by including at least 85% of the participating mass, and a uniform acceleration distribution proportional to the storey masses. This approach allows both the predominant translational response and the influence of torsional effects to be considered within the assumptions of the adopted nonlinear static procedure. For both principal directions, the uniform distribution proved to be the most demanding loading condition. The main analysis parameters for the X direction are listed in Table 2, while the bilinear capacity curve and displacement demands are shown in the ADRS for the Life Safety Earthquake (LSE), with a return period of 475 years, and the Collapse Prevention Earthquake (CPE), with a return period of 975 years (Fig. 13b). For both LSE and CPE, the equal displacement rule was used to compute the displacement demands, as the period of the SDOF structure is greater than T_C. This analysis indicates that the existing structure does not meet the displacement requirements at both LSLS and CPLS in the two main directions; therefore, a retrofit intervention is necessary.

5.2. Design of the retrofit system

The required number of panels to enhance the seismic performance of the reference case study building was determined using the design methodology described in 4. The first step of the procedure involved defining the seismic input: the horizontal response spectrum at the significant damage limit state, with a behaviour factor of 1.5, was derived for Toscolano Maderno for soil type C, and a nominal life of 50 years, in accordance with NTC18. The maximum horizontal acceleration, corresponding to the plateau value, was 0.383 g. The tributary loads on the 1st, 2nd, and 3rd floors were 1517 kN, 1466 kN, and 802 kN, respectively. The seismic base shear force F_b was 616 kN in both directions, with corresponding inertia forces of 491 kN and 225 kN at the 2nd and 3rd stories, respectively. The number of panels to be installed on each façade was determined by maximizing the use of the available free surface area while ensuring architectural compatibility with existing openings such as windows and doors. The panel layout on the reference plan is shown in Fig. 14, where the installed panels are indicated in blue and the windows that will be partially or fully covered are highlighted in red. This occurs only at the first storey and involves

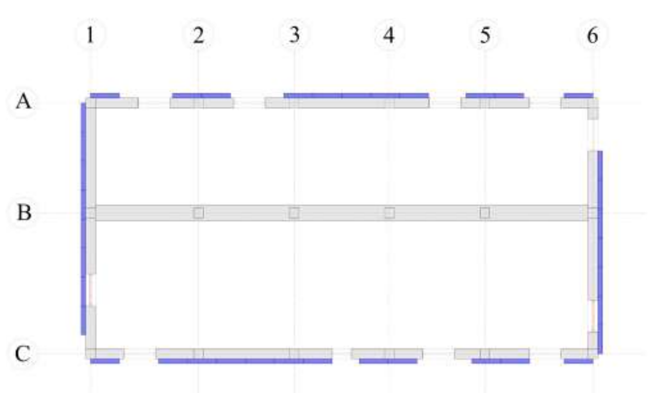

Fig. 14. Disposition of the panels.

Table 3
Definition of the geometry of the necessary panels for the case study building. Note: "S-" and "D-" stands for single and double panels configuration.

Façade	n°panels	Sheet thickness (mm) and type		
		1st storey	2nd storey	3rd storey
X_left (1)	8	D−1.5	D−1.3	S−1.2
X_right (6)	7	D−1.5	D−1.3	S−1.2
Y_top (A)	12	S−1.8	S−1.5	S−1
Y_bottom (C)	11	S−1.8	S−1.5	S−1

only the windows of the basement storage rooms. Given the secondary function of these spaces and the limited impact on natural lighting and ventilation requirements, this configuration is considered acceptable and does not present significant issues from an architectural or functional standpoint. Once the number of panels was defined, the required thickness of the perforated steel sheet was determined by evaluating the panel resistance using the analytical formulation presented in 3.1.2. This phase of the design procedure is summarized in Table 3, which outlines the panel distribution and the corresponding thicknesses for each façade. In some cases, a double panel sandwich-type configuration was selected to maximize the resistance of the shear wall.

The capacity curves of the retrofit system were derived for both principal directions of the building following the analytical procedure described in 4.2. This resulted in equivalent stiffness values k_2 equal to 100800 kN/m and 92840 kN/m, and system capacities R_{sys} equal to 1363 kN and 1380 kN for the X and Y directions, respectively. The global structural performance was subsequently evaluated in the ADRS domain, showing that interstorey drift demand remained below the 0.3% target limit. These results indicate that the adopted retrofit configuration provides a satisfactory balance between lateral stiffness and strength within the assumptions of the proposed analytical procedure.

Finally, the SPM was employed to evaluate the axial forces in the studs, with the results reported in Table 4. The buckling resistance of the compressed vertical studs, consisting of built-up cold-formed cross sections, was evaluated in accordance with the provisions of the European codes [44], considering Class 4 profiles. The resulting buckling resistance was 240 kN, which is lower than the demand on the most heavily loaded studs. Therefore, the area and second moment of inertia of the non-compliant studs were increased to achieve the required capacity.

5.3. Numerical analysis of the retrofitted structure

Starting from the numerical model of the existing structure, the retrofit system was integrated by incorporating shear panels according to the number, position, and mechanical properties defined during the design phase. The retrofit panels were modelled through the simplified Model C described in 3.3, calibrated to reproduce the global stiffness and strength response of the panel system as a function of both the steel sheet thickness and the flexural stiffness of the adopted vertical studs. To ensure accurate numerical simulation of the connections between the structural elements, the panel model heights, originally set at 2.73 m, were adjusted to match the actual interstorey heights: 2.6 m for the first storey and 3.1 m for the second and third floors. The internal elements of Model C were calibrated accordingly to maintain correct structural behaviour despite the height variation. This calibration was essential to accurately reproduce the structural response and to avoid the need for additional vertical connections between panels installed on different floors. Each panel was therefore rigidly connected to the corresponding horizontal beam of the existing reinforced concrete frame. A detailed investigation of the actual mechanical behaviour of the panel-to-frame connections is beyond the scope of this study. The FE model of the retrofitted structure is shown in Fig. 15.

Nonlinear static analyses were performed and the retrofitted building was assessed in both directions using the N2 method [48]. Nonlinear

Table 4
Application of the stringer-panel model to the panels. Note: a= 0.91 m and h= 2.73 m for all panels.

Façade	n°panels	Shear flow (kN/m)			Forces in cross-rails (max.) (kN)			Forces in vertical studs (max.) (kN)		
		f_3	f_2	f_1	N_{h3}	N_{h2}	N_{h1}	N_{v3}	N_{v2}	N_{v1}
X_left	8	32	69	87	29	63	79	87	276	514
X_right	7	36	79	100	33	72	91	99	316	587
Y_top	12	21	46	58	19	42	53	58	184	343
Y_bottom	11	23	50	63	21	46	58	63	201	374

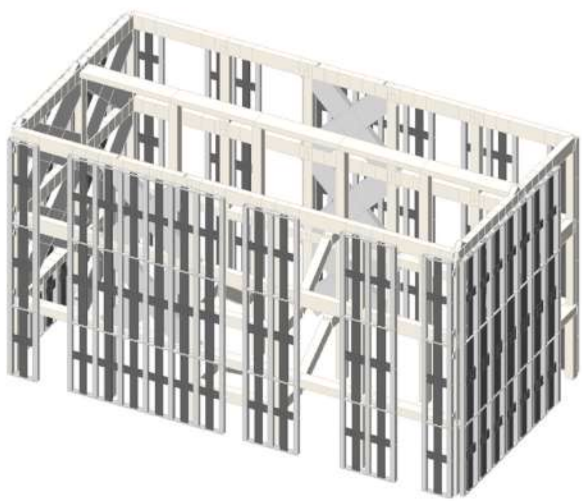

Fig. 15. Finite element model of the retrofitted buildings with RC elements, masonry infills and CFS panels with the proposed modelling strategy.

Table 5
Modal properties of the building before and after the retrofit application.

Mode	Before retrofit				After retrofit			
	T (s)	*Modal participation masses (%)*			*T (s)*	*Modal participation masses (%)*		
		UX	*UY*	*RZ*		*UX*	*UY*	*RZ*
1	0.37	37	37	19	0.25	1	87	1
2	0.34	31	50	7	0.23	78	1	12
3	0.23	24	67	67	0.16	12	0	78

Table 6
N2 method main parameters for the retrofitted structure for the X direction.

Parameter	Symbol	Unit	Value
Participation factor	Γ	(-)	1
Mass of the equivalent SDOF system	m	kN/g	401
Fundamental period of the equivalent SDOF system	T_1	s	0.30
Stiffness of the equivalent SDOF system	k_1	kN/m	169000
Yielding force of the bilinear curve	F_{y1}	kN	2027
Yielding displacement of the bilinear curve	d_{y1}	m	0.012
Displacement capacity of the SDOF system for the Life Safety (LS) limit state	d_c^{LS}	m	0.033
Displacement capacity of the SDOF system for the Collapse Prevention (CP) limit state	d_c^{CP}	m	0.044
Displacement demand for the SDOF system for the LS limit state	d_d^{LS}	m	0.013
Displacement demand for the SDOF system for the CP limit state	d_d^{CP}	m	0.017

static analyses were performed and the retrofitted building was assessed in both directions using the N2 method [49]. In accordance with NTC 2018, both a principal modal load pattern and a secondary uniform acceleration distribution were considered. As observed for the original building, the uniform distribution proved to be the most demanding loading condition for the retrofitted configuration. The dynamic properties of the building before and after the retrofit intervention are summarized in Table 5. The retrofit system significantly increased the global lateral stiffness and modified the modal response of the structure. In particular, the translational participating mass increased up to 87% in the Y direction and 78% in the X direction, while the influence of torsional effects was reduced compared to the original configuration. Consequently, the retrofitted building exhibited a more regular and predominantly translational dynamic response, supporting the applicability of the adopted nonlinear static analysis procedure.

The equivalent SDOF parameters derived through the N2 procedure for the retrofitted structure are summarized in Table 6. The reduction of the equivalent period T_1 is consistent with the increase in the equivalent lateral stiffness k1 induced by the retrofit system.

The application of the retrofit solution led to an increase in both lateral stiffness and strength (Fig. 16a). Moreover, the retrofit intervention substantially reduced the interstorey drift demand along the building height (Fig. 16b). The target interstorey drift limit of 0.3% at the LSLS was satisfied in both principal directions, confirming the effectiveness of the proposed design procedure.

Fig. 17 presents the vulnerability assessment of the retrofitted structure in the X direction, while Table 7 summarizes the corresponding analysis results. Following the intervention, the building was verified in both directions for all considered earthquake scenarios. A comparison of the damage states at different limit state demands before and after the application of the panels (Table 7 and Table A4 in Appendix) demonstrates that the retrofit solution effectively limits damage to both structural and non-structural elements at the serviceability limit states. At ultimate limit states, some of the applied panels experience plasticization, contributing to seismic energy dissipation and requiring replacement. At LSLS, which governs the retrofit design, 10 panels in the X direction (9% of the total) and 19 panels in the Y direction (17%) exceeded the first yielding point of the trilinear skeleton curve.

6. Conclusions

In this work, the effectiveness of cold-formed steel panels with burring holes for the integrated renovation of existing reinforced concrete buildings was assessed. Originally developed and tested in Japan as lateral force-resisting systems for new constructions, these panels have been adapted here for seismic strengthening applications. The proposed retrofit system is prefabricated, standardized, and demountable, which facilitates rapid installation, reduces costs, and allows disassembly and reuse at the end of a building's service life, thereby enhancing overall sustainability.

Three numerical models were developed to reproduce the monotonic

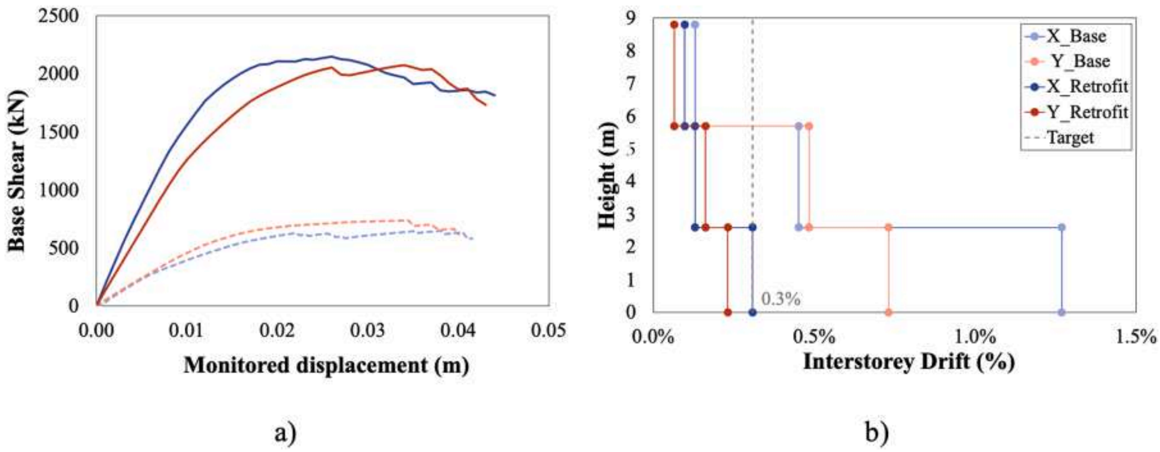

Fig. 16. a) Capacity curves of the building before (Base) and after (Retrofit) the retrofit intervention and b) interstorey drift ratios at LSLS.

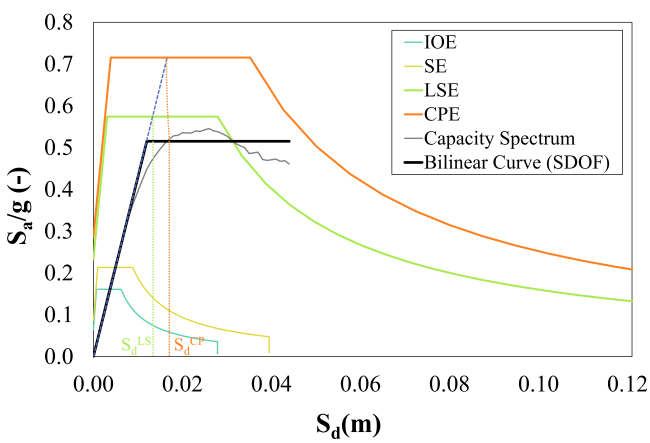

Fig. 17. Seismic vulnerability assessment of the retrofitted structure in the X direction in the ADRS for various limit states with their return period.

behaviour observed in previous experimental tests. Model A, developed in Simulia Abaqus, was the most refined and fully accounted for geometric nonlinearities, though this required significant computational effort. Beginning with the 1.2 mm sheet thickness configuration, a parametric analysis was conducted to derive capacity curves for panels of different thicknesses, and a regression analysis produced a practical formula for estimating wall resistance and elastic stiffness as a function of sheet thickness. Model B, implemented in MidasGen, used plate and beam elements with calibrated connections; the position and number of connections were adjusted to match the experimental monotonic capacity curve, as this model did not include geometric nonlinear effects. Model C, the most simplified, consisted solely of beam elements. Specifically, the steel sheet was idealized as two sets of beam elements with calibrated plastic hinges to reproduce the nonlinear response, while the frame elements were modelled as pin-connected beams, so they did not contribute to the lateral resistance of the panel. This simplification made Model C highly computationally efficient and suitable for practical design applications.

A design methodology for retrofit interventions using these walls was proposed. Based on a spectral analysis at the Life Safety Limit State and

Table 7
Seismic vulnerability analysis results by the N2 method before and after the retrofit intervention.

Limit state	Roof Drift Ratio: Capacity (demand)		Damage assessment	
	Before retrofit	*After retrofit*	*Before retrofit*	*After retrofit*
X direction				
IOLS	0.106% (0.114%)	0.09% (0.03%)	Yielding[1] in 5 columns (5%)	No yielding
SLS	0.159% (0.165%)	0.14% (0.06%)	Yielding in 9 columns (17%)	Yielding in 2 columns (4%)
LSLS	0.35% (0.44%)	0.38% (0.15%)	Yielding in 20 columns (37%) Ultimate resistance[2] in 7 columns (13%) Cracking in 2 infills (17%)	Yielding in 21 columns (39%) First yielding[3] of 11 panels (9%) Elastic infills
CPLS	0.47% (0.56%)	0.50% (0.22%)	Partial collapse mechanism development at the ground storey Cracking in 2 infills (17%)	Yielding in 33 columns (61%) First yielding of 24 panels (23%) Elastic infills
Y direction				
IOLS	0.110% (0.111%)	0.12% (0.06%)	Yielding in 4 columns (7%)	No yielding
SLS	0.165% (0.170%)	0.18% (0.08%)	Yielding in 14 columns (26%)	Yielding in 2 columns (4%)
LSLS	0.34% (0.42%)	0.37% (0.21%)	Yielding in 34 columns (63%) Maximum resistance[5] in 1 infill	Yielding in 52 columns (96%) First yielding of 19 panels (17%) Elastic infills
CPLS	0.45% (0.52%)	0.49% (0.28%)	Failure[6] of 12 columns (22%) Ultimate resistance in 4 columns (7%) Maximum resistance in 1 infill	Yielding in 52 columns (96%) First yielding in 30 panels (26%) Cracking in 1 infill

[1] Point B in Fig. 12a (ϑ_y).
[2] Point D in Fig. 12a (strength loss).
[3] First yielding point of the trilinear curve that characterizes the nonlinear behaviour of Model C of panels.
[4] First yielding point of the masonry infills (Fig. 12c).
[5] Point (F_m, Δ_m) in Fig. 12c.
[6] Point E in Fig. 12a, ultimate deformation for the plastic hinge.

the equivalent lateral force method of Eurocode 8, it enables determination of the number and thickness of panels per façade through an iterative procedure based on the relative stiffness of the existing building and retrofit configuration. Verification of studs and cross-rails can be performed using the stringer-panel model, which decomposes planar elements into a plane element subjected to constant shear flows and linear elements subjected to varying normal forces. The retrofit solution, based on cold-formed steel panels with burring holes, was designed and applied to the case study building following the developed methodology. Detailed vulnerability assessments were conducted before and after the intervention, allowing direct comparison of the building's seismic performance. The analyses showed that, after the retrofit, the structure meets the requirements for both serviceability and ultimate limit states. Specifically, damage to structural and non-structural components is prevented at the serviceability limit state, ensuring the building remains operational after design-level seismic events. Moreover, the retrofit system effectively regularized the structural response.

These findings confirm both the effectiveness of the proposed CFS panel system in enhancing seismic safety and the reliability and applicability of the design procedure for practical engineering use. The case study demonstrates how this retrofit approach can transform an inherently vulnerable reinforced concrete building into a seismically robust structure while maintaining high levels of sustainability, constructability, and cost efficiency.

Novelty

This study advances the field of seismic retrofitting and sustainable renovation through several original contributions. First, it introduces the use of cold formed steel panels with burring holes, originally developed in Japan for new constructions, as an innovative dry assembled seismic strengthening solution for existing reinforced concrete buildings. In contrast to conventional invasive techniques, the proposed system is prefabricated, fully demountable and reusable, thereby combining structural reliability with Life Cycle Thinking principles.

A further contribution lies in the development of a comprehensive multi scale modeling and design framework. The study proposes three complementary numerical strategies of increasing simplification: a refined three-dimensional finite element model capturing geometric nonlinearities, an intermediate macro element approach, and a simplified beam-based model tailored to professional engineering practice. A parametric study enabled the derivation of a new regression formula that estimates wall resistance as a function of steel sheet thickness, providing a practical design aid.

To facilitate real world application, the paper establishes a design methodology fully aligned with the European building codes for determining the global retrofit requirements. It also extends the analytical use of the stringer-panel analogy to verify studs and cross rails by resolving the complex panel stress field into tractable shear flows and axial forces.

The methodology is validated through a real case study, demonstrating that the strengthened structure satisfies both Serviceability and Ultimate Limit State requirements. Overall, this work delivers a holistic and experimentally grounded framework that enhances the seismic performance of vulnerable buildings while emphasizing constructability, reversibility and environmental sustainability.

CRediT authorship contribution statement

Michelle Gualdi: Writing – review & editing, Writing – original draft, Visualization, Validation, Software, Methodology, Investigation, Formal analysis. **Andrea Belleri:** Writing – review & editing, Validation, Supervision, Resources, Project administration, Methodology, Investigation, Funding acquisition, Conceptualization. **Simone Labò:** Writing – review & editing, Validation, Methodology, Investigation. **Atsushi Sato:** Writing – review & editing, Validation, Resources, Methodology, Investigation, Funding acquisition, Data curation.

Funding

This research did not receive any specific grant from funding agencies in the public, commercial, or not-for-profit sectors.

Declaration of Competing Interest

The authors declare that they have no known competing financial interests or personal relationships that could have appeared to influence the work reported in this paper.

Appendix

This appendix provides supplementary information related to the numerical modelling and structural response of the RC case study building with masonry infills presented in Section 5. Tables A1 and A2 report the geometrical and reinforcement details of the RC columns and beams, respectively. Table A3 summarizes the modelling parameters adopted for the constitutive skeleton curve of the masonry infills. Finally, Table A4 complements the discussion of the nonlinear analysis results by presenting the distribution of plastic hinges in the RC elements of the existing building before and after the retrofit intervention.

Table A1
Columns detailing, with reference to Fig. 11. Note: Stirrups Φ6/120 mm

Column ID	Lx (mm)	Ly (mm)	Longitudinal rebars
1st floor			
All	300	300	4Φ12
2nd and 3rd floor			
1, 6, 13, 18	250	250	4Φ10
2–5, 14–17	250	300	4Φ10
8–11	300	300	4Φ12

Table A2
Beams detailing, with reference to Fig. 11

Beam ID	B (mm)	H (mm)	Longitudinal rebars		Stirrups
			i	j	
1st floor					
1–7, 6–12	400	300	2Φ8 + 2Φ10 top 2Φ10 bottom	2Φ8 + 2Φ10 top 2Φ10 bottom	2LΦ6/300
7–13, 12–18	400	300	2Φ8 + 2Φ12 top 2Φ12 bottom	2Φ8 + 2Φ10 top 2Φ10 bottom	2LΦ6/300
1–2, 5–6, 13–14, 17–18	400	300	2Φ8 + 2Φ12 top 3Φ12 bottom	2Φ8 + 6Φ12 top 3Φ10 bottom	2LΦ8/250
2–3, 4–5, 14–15, 16–17	400	300	2Φ8 + 6Φ12 top 3Φ10 bottom	2Φ8 + 4Φ12 top 3Φ10 bottom	2LΦ8/250
3–4, 15–16	400	300	2Φ8 + 4Φ12 top 3Φ10 bottom	2Φ8 + 4Φ12 top 3Φ10 bottom	2LΦ8/250
7–8, 11–12	600	190	2Φ8 + 4Φ14 top 4Φ14 bottom	2Φ8 + 6Φ14 top 4Φ14 bottom	4LΦ8/200
8–9, 10–11	600	190	2Φ8 + 6Φ14 top 4Φ14 bottom	2Φ8 + 4Φ14 top 4Φ14 bottom	4LΦ8/200
9–10	600	190	2Φ8 + 4Φ14 top 4Φ14 bottom	2Φ8 + 4Φ14 top 4Φ14 bottom	4LΦ8/200
2nd and 3rd floor					
1–7, 6–12	250	500	2Φ8 + 2Φ10 top 2Φ10 bottom	2Φ8 + 2Φ10 top 2Φ10 bottom	2LΦ8/300
7–13, 12–18	250	500	2Φ8 + 2Φ12 top 2Φ12 bottom	2Φ8 + 2Φ10 top 2Φ10 bottom	2LΦ6/300
1–2, 5–6, 13–14, 17–18	250	500	2Φ8 + 2Φ10 top 2Φ10 bottom	2Φ8 + 6Φ10 top 2Φ10 bottom	2LΦ8/300
2–3, 4–5, 14–15, 16–17	250	500	2Φ8 + 6Φ10 top 2Φ10 bottom	2Φ8 + 4Φ120top 2Φ10 bottom	2LΦ8/300
3–4, 15–16	250	500	2Φ8 + 4Φ10 top 2Φ10 bottom	2Φ8 + 4Φ120top 2Φ10 bottom	2LΦ8/300
7–8, 11–12	600	190	2Φ8 + 4Φ14 top 4Φ14 bottom	2Φ8 + 6Φ14 top 4Φ14 bottom	4LΦ8/200
8–9, 10–11	600	190	2Φ8 + 6Φ14 top 4Φ14 bottom	2Φ8 + 4Φ14 top 4Φ14 bottom	4LΦ8/200
9–10	600	190	2Φ8 + 4Φ14 top 4Φ14 bottom	2Φ8 + 4Φ14 top 4Φ14 bottom	4LΦ8/200

Table A3
Modelling parameters of the equivalent diagonal struts for masonry infills

Infill dimensions	Eq. Area m^2	F_y kN	F_m kN	F_r kN	Δ_y mm	Δ_m mm	Δ_r mm
3 × 2.6 m	0.1796	108	134	47	5.83	9.72	36.14
3 × 3.1 m	0.1656	118	147	52	6.34	1.56	39.29
3.45 × 2.6 m	0.2032	119	148	52	6.16	10.27	38.22
3.45 × 3.1 m	0.1822	127	159	56	6.84	11.4	42.42
4.425 × 3.1 m	0.2264	150	188	66	7.61	12.68	47.17

Table A4
Plastic hinge distribution in the RC beams and columns of the case study building before and after the application of the retrofit solution. The colour scale ranges from blue (linear elastic behaviour) to red (failure), with intermediate levels B, C, D represented by cyan, yellow and orange, respectively, corresponding to the points in Fig. 12a

IOLS	
X_Before retrofit	***X_After retrofit***
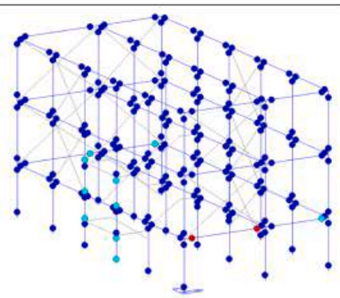	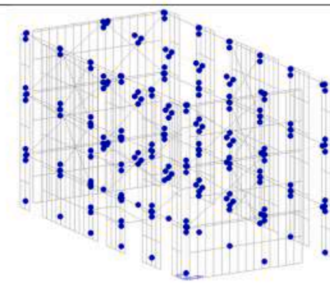
Y_Before retrofit	***Y_After retrofit***
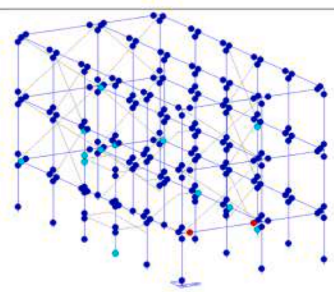	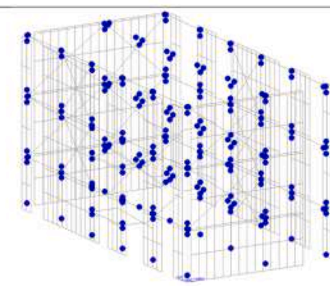
SLS	
X_Before retrofit	***X_After retrofit***
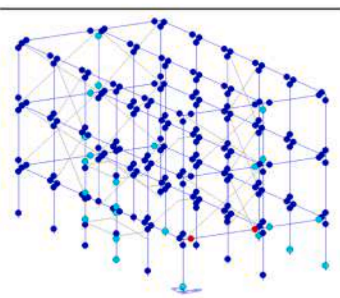	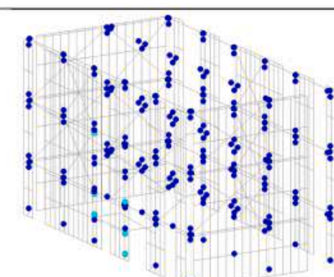
Y_Before retrofit	***Y_After retrofit***
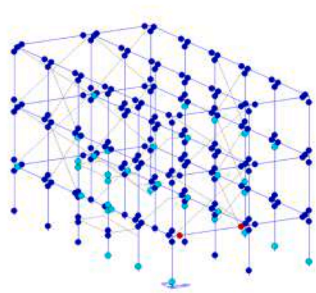	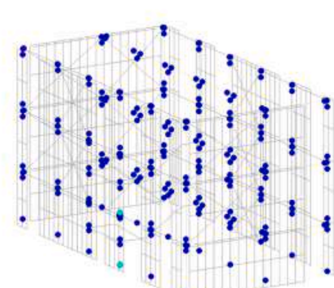

(*continued on next page*)

Table A4 (*continued*)

LSLS	
X_Before retrofit	*X_After retrofit*
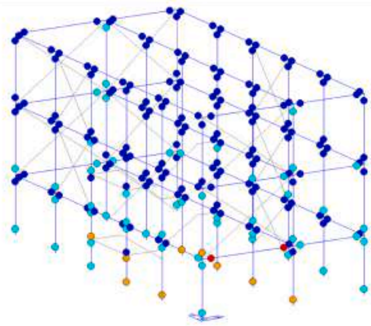	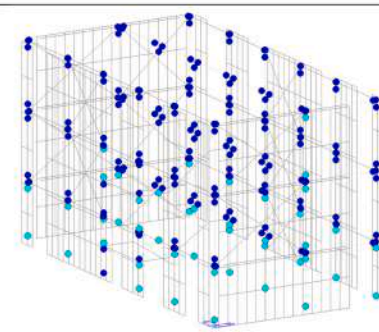
Y_Before retrofit	*Y_After retrofit*
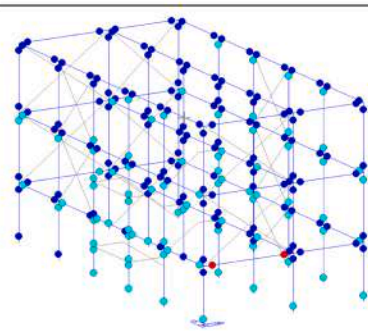	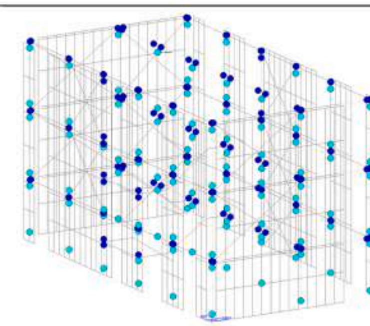
CPLS	
X_Before retrofit	*X_After retrofit*
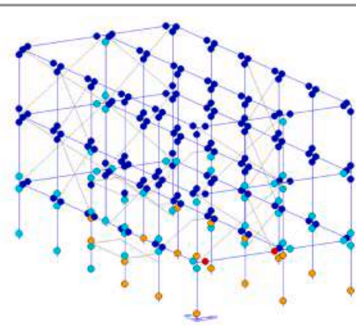	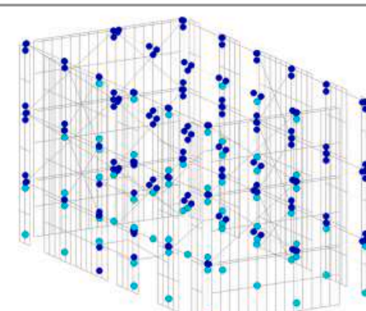
Y_Before retrofit	*Y_After retrofit*
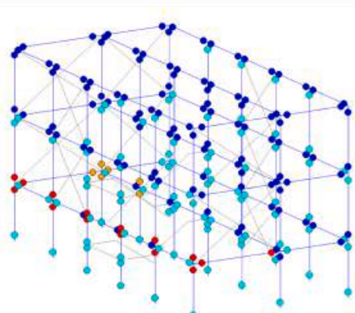	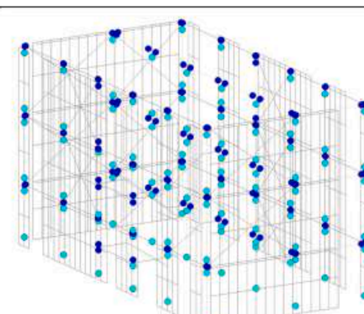

Data availability

Data will be made available on request.

References

[1] United Nations Environment Programme. Global Status Report for Buildings and Construction: Beyond foundations: Mainstreaming sustainable solutions to cut emissions from the building sector. Nairobi 2024.
[2] Italian Civil Protection Department. Overview of the potential major disasters in Italy. National Risk Assessment; 2018.
[3] Ferreira J, Duarte Pinheiro MD, De Brito J. Economic and environmental savings of structural buildings refurbishment with demolition and reconstruction - A Portuguese benchmarking. J Build Eng 2015;3:114–26. https://doi.org/10.1016/j.jobe.2015.07.001.
[4] Marique AF, Rossi B. Cradle-to-grave life-cycle assessment within the built environment: comparison between the refurbishment and the complete reconstruction of an office building in Belgium. J Environ Manag 2018;224: 396–405. https://doi.org/10.1016/j.jenvman.2018.02.055.
[5] Pittau F, Giacomel D, Iannaccone G, Malighetti L. Environmental consequences of refurbishment versus demolition and reconstruction: a comparative life cycle assessment of an Italian case study. J Green Build 2020;15(4):155–72. https://doi.org/10.3992/jgb.15.4.155.
[6] Belleri A, Marini A. Does seismic risk affect the environmental impact of existing buildings? Energy Build 2016;110:149–58. https://doi.org/10.1016/j.enbuild.2015.10.048.
[7] Marini A, Passoni C, Belleri A, Feroldi F, Preti M, Metelli G, Riva P, Giuriani E, Plizzari G. Combining seismic retrofit with energy refurbishment for the sustainable renovation of RC buildings: a proof of concept. Eur J Environ Civil Eng 2017. https://doi.org/10.1080/19648189.2017.1363665.
[8] Passoni C, Marini A, Belleri A, Menna C. Redefining the concept of sustainable renovation of buildings: state of the art and an LCT-based design framework. Sustain City Soc 2021;64:102519. https://doi.org/10.1016/j.scs.2020.102519.
[9] World Bank, Investment in Disaster Risk Management in Europe Makes Economic Sense. 2021. https://doi.org/10.1596/35686.
[10] Labò S, Passoni C, Marini A, Belleri A. Design of diagrid exoskeletons for the retrofit of existing RC buildings. Eng Struct 2020;220:1–20. https://doi.org/10.1016/j.engstruct.2020.110899.
[11] Zanni J, Cademartori S, Marini A, Belleri A, Passoni C, Giuriani E, Riva P, Angi B, Brumana G, Marchetti AL. Integrated deep renovation of existing buildings with prefabricated shell exoskeleton. Sustainability 2021;13:11287. https://doi.org/10.3390/su132011287.
[12] Margani G, Evola G, Tardo C, Marino EM. Energy, seismic, and architectural renovation of RC framed buildings with prefabricated timber panels. Sustainability 2020;12:4845. https://doi.org/10.3390/su12124845.
[13] Sustersic I, Dujic B. Seismic strengthening of existing concrete and masonry buildings with crosslam timber panels. In: Aicher S, et al., editors. Materials and Joints in Timber Structures. 9. RILEM Bookseries; 2014. https://doi.org/10.1007/978-94-007-7811-5_64.
[14] Dalla Mora T, Righi A, Peron F, Romagnoni P. Functional, energy and seismic retrofitting in existing buildings: an innovative system based on xlam technology. Energy Procedia 2015;82:486–92. https://doi.org/10.1016/j.egypro.2015.11.851.
[15] Prota A., Tartaglia R., Di Lorenzo G., Landolfo R. Seismic strengthening of isolated RC framed structures through orthogonal steel exoskeleton: Bidirectional non-linear analyses. Eng Struct 302:117496. https://doi.org/10.1016/j.prostr.2024.09.395.
[16] Misawa Y, Azuma K, Cho W, Iwamoto S, Iwata M. Simulation study on energy conservation performance for integrated external louver facades. J Facade Des Eng 2015;3:237–52. https://doi.org/10.7480/jfde.2015.3-4.993.
[17] Casprini E., Belleri A., Marini A., Labò A., Passoni C. Pin-supported walls as seismic retrofit for existing RC frames: feasibility and preliminary design. Bull Earth Eng 20:5349–5381. https://doi.org/10.1007/s10518-022-01405-z.
[18] Casprini E., Belleri A., Marini A., Passoni C., Labò S. Pin-supported walls as seismic retrofit for existing RC frames: performance improvement through link removal. Bull Earth Eng 21:2817–2844. https://doi.org/10.1007/s10518-023-01628-8.
[19] Landolfo R, Fiorino L, Della Corte G. Seismic behavior of sheathed cold-formed structures: physical tests. J Struct Eng 2006;132(4):570–81. https://doi.org/10.1061/(ASCE)0733-9445(2006)132:4(570).
[20] Dubina D. Behavior and performance of cold-formed steel-frames houses under seismic action. J Constr Steel Res 2008;64:896–913. https://doi.org/10.1016/j.jcsr.2008.01.029.
[21] Serrette R, Ogunfunmi K. Shear resistance of gypsum-sheathed light-gauge steel stud walls. J Struct Eng 1996;122(4):383–9. https://doi.org/10.1061/(ASCE)0733-9445(1996)122:4(383).
[22] Terracciano G, Di Lorenzo G, Formisano A, Landolfo R. Cold-formed thin-walled steel structures as vertical addition and energetic retrofitting systems of existing masonry buildings. Eur J Environ Civil Eng 2014. https://doi.org/10.1080/19648189.2014.974832.
[23] Davino A, Longobardi G, Meglio E, Dallari A, Formisano A. Seismic energy upgrading of an existing brick masonry building by a cold-formed steel envelope system. Buildings 2022;12:1918. https://doi.org/10.3390/buildings12111918.
[24] Formisano A, Galano S, Meglio E, Del Vecchio C, Prota A. Experimental investigation on innovative lightweight steel exoskeleton for seismic resilience of masonry-infilled reinforced concrete frames. Eng Struct 2025;344:121410. https://doi.org/10.1016/j.engstruct.2025.121410.
[25] Demirel IO, Galano S, Morandi P, Akyuz U. Seismic enhancement of masonry-infilled substandard reinforced concrete frames using lightweight steel exoskeleton. Earthq Eng Struct Dyn 2025;55(3):603–23. https://doi.org/10.1002/eqe.70102.
[26] Kawai Y, Tohnai S, Tanaka H, Sato A, Ono T. Shear resistance mechanisms of steel sheet walls with burring holes: shear stiffness and large deformation behavior. J Struct Constr Eng 2019;84(757):437–46. https://doi.org/10.3130/aijs.84.437.
[27] Kawai Y, Fujihashi K, Tohnai S, Sato A, Ono T. Continuous high-panelized steel sheet shear walls with burring holes and the effect of vertical slits. AIJ J Technol Des 2018;24(58):1041–6. https://doi.org/10.3130/aijt.24.1041.
[28] Kawai Y, Fujihashi K, Tohnai S, Sato A, Ono T. Shear resistance mechanisms on high-panelized steel sheet shear walls with burring holes. AIJ J Technol Des 2018; 24(56):177–82. https://doi.org/10.3130/aijt.24.177.
[29] Kawai Y, Tohnai S, Kaibara H, Sato A, Ono T. Shear resistance mechanisms of high-panelized sheet walls with burring holes. J Struct Constr Eng 2020;85(768): 275–85. https://doi.org/10.3130/aijs.85.275.
[30] Gualdi M. Belleri A., Marini A., Labò S., Rota L. 2025. Preliminary assessment of self-centering rocking steel systems for lightweight buildings. In: 10th ECCOMAS Thematic Conference on Computational Methods in Structural Dynamics and Earthquake Engineering (COMPDYN 2025), Rhodes Island, Greece, 15-18 June 2025. https://dx.doi.org/10.7712/120125.12704.25154.
[31] Gualdi M., Belleri A., Marini A., Labò S., Preliminary assessment of self-centring steel frame systems with energy dissipation devices. In: XX Convegno di Ingegneria Sismica, Assisi, Italy, 07-11 September 2025. https://dx.doi.org/10.1016/j.prostr.2025.12.027.
[32] European Committee for Standardization (CEN), Eurocode 8: Earthquake resistance design of structures, 2006.
[33] Landolfo R, Shakeel S, Fiorino L. Lightweight steel systems: proposal and validation of seismic design rules for second generation of Eurocode 8. Thin-Walled Struct 2022;172:108826. https://doi.org/10.1016/j.tws.2021.108826.
[34] Dassault Systems, Abaqus Documentation, 2020.
[35] MidasGen. Analysis Manual for Midas GEN; 2024.
[36] Gualdi M., Belleri A., Labò S., Marini A., Sato A., FE Models of Cold-Formed Steel Panels with Burring Holes for the Seismic Retrofit of Existing Buildings. In: 11th International Conference on Behaviour of Steel Structures in Seismic Areas (STESSA 2024), Salerno, Italy, 8-10 July, 2024. https://dx.doi.org/10.1007/978-3-031-62888-7_69.
[37] Mehrabi AB, Benson SP, Schuller MP, Noland JL. Experimental evaluation of masonry-infilled RC frames. J Struct Eng 1996;122(3):228–37. https://doi.org/10.1061/(ASCE)0733-9445(1996)122:3(228).
[38] Wagner H., Flat Sheet Metal Girders with Very Thin Metal Web Part I General Theories and Assumptions. National Advisory Committee for Aeronautics, Technical Memorandum n. 604, 1929. https://digital.library.unt.edu/ark:/67531/metadc63634/m1/6/.
[39] Khun P, Peterson JP, Levin LR. A summary of diagonal tension part I - methods of analysis. National Advisory Committee for Aeronautics, Technical Note 1952;2661. http://hdl.handle.net/2060/19930083335.
[40] Khun P., Peterson J.P., Levin L.R., A summary of diagonal tension part II - experimental evidence. National Advisory Committee for Aeronautics, Technical Note 2661, 1952.https://ntrs.nasa.gov/citations/19930083352.
[41] Nielsen PM, Linh HC. Limit Analysis and concrete plasticity. CRS press; 1984.
[42] Kamiya F, Itani RY. Design of wood diaphragms with openings. J Struct Eng 1998; 124(7):839–48. https://doi.org/10.1061/(ASCE)0733-9445(1998)124:7(839).
[43] Godinez SE, Restrepo JI. Stringer-panel model to support the seismic design and response verification of building diaphragms. Resilient Cities Struct 2023;2:46–67. https://doi.org/10.1016/j.rcns.2023.02.003.
[44] European Committee for Standardization (CEN) Eurocode 3: Design of steel structures, 2006 .
[45] Morandi P, Hak S, Magenes G. Comportamento sismico delle tamponature in laterizio in telai in c.a.: definizione dei livelli prestazionali e calibrazione di un modello numerico. XIV Convegno di Ing Sismica ANIDIS Bari 2011.
[46] Italian Ministry of Infrastructure and Transport: Technical Standards for Construction (NTC 2018), Rome, Italy, 2018.
[47] Decanini L., Gavarini C., Bertoldi S., Telai tamponati soggetti ad azioni sismiche, un modello semplificato: confronto sperimentale e numerico. In: VI Convegno Nazionale di Ingegneria Sismica in Italia, Perugia; 1993.
[48] Sassun K, Sullivan TJ, Morandi P, Cardone D. Characterising the in-plane seismic performance of infill masonry. Bull NZ Soc Earthq Eng 2016;49(1):98–115. https://doi.org/10.5459/bnzsee.49.1.98-115.
[49] Fajfar P. A nonlinear analysis method for performance-based seismic desig. Earthq Spectra 2000;16(3):573–92. https://doi.org/10.1193/1.1586128.